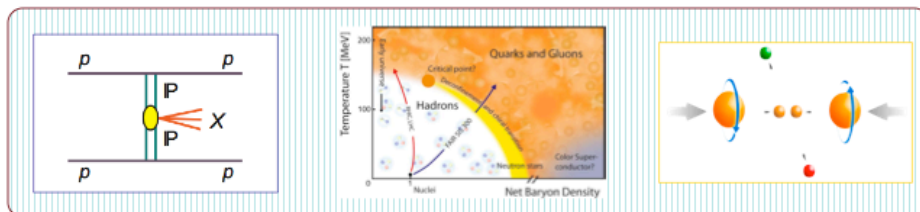
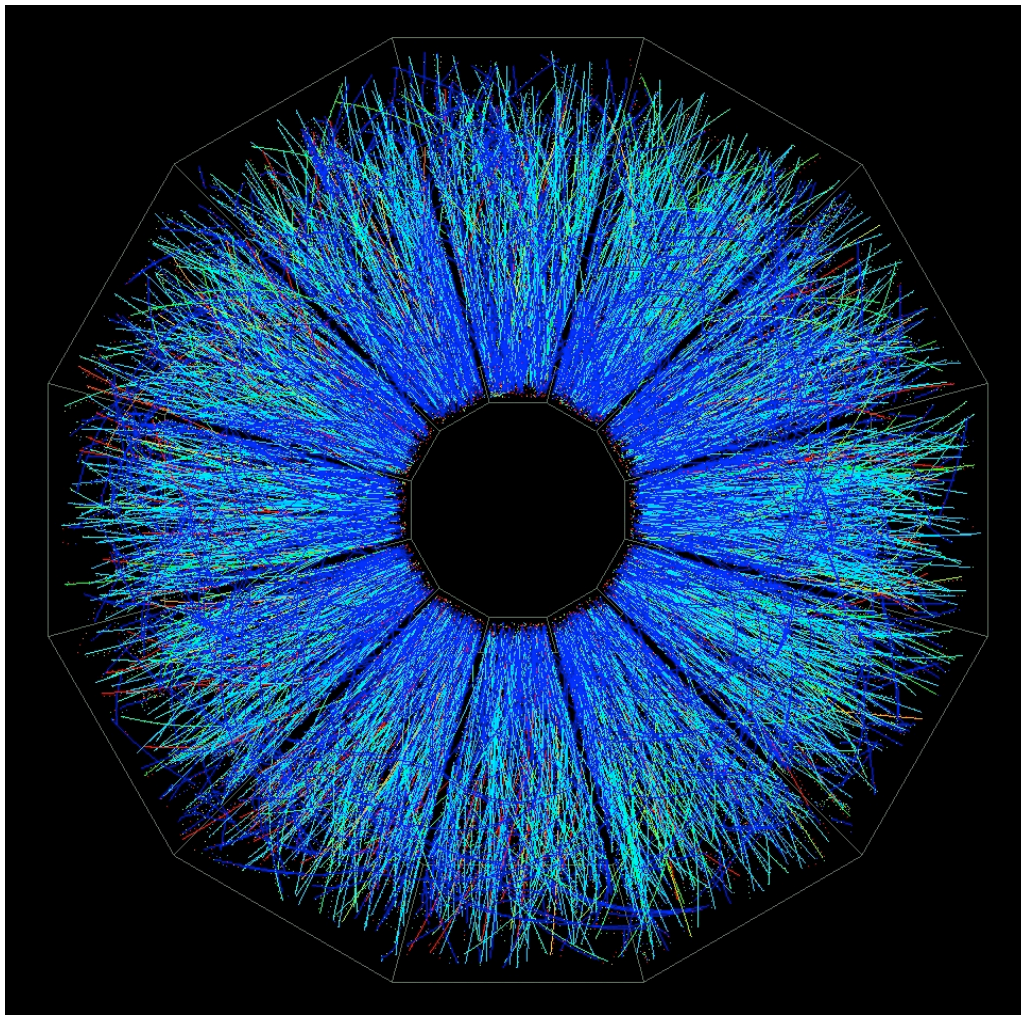


# RHIC Beam Use Request For Runs 13 and 14

The STAR Collaboration  
May 28, 2012



## Table of Contents

<b>1. Executive Summary</b> .....	<b>3</b>
<b>2. Report on Run 12 Performance</b> .....	<b>6</b>
<b>2.1 Introduction</b> .....	<b>6</b>
<b>2.2 Run 12 U+U Collisions</b> .....	<b>6</b>
<b>2.3 The FGT Performance</b> .....	<b>8</b>
<b>3. Study of p+p Collisions</b> .....	<b>12</b>
<b>3.1 Overview</b> .....	<b>12</b>
<b>3.2 Recent Highlights from the STAR Spin Program</b> .....	<b>13</b>
<b>3.3 Summary of Run 12 Polarized Proton Collisions</b> .....	<b>18</b>
<b>3.4 Run 13 Request for 500 GeV p+p Collisions</b> .....	<b>20</b>
<b>3.5 Run 14 Request for 200 GeV p+p Collisions</b> .....	<b>27</b>
<b>4. Physics with Tagged Forward Protons at STAR</b> .....	<b>29</b>
<b>4.1 Executive Summary</b> .....	<b>29</b>
<b>4.2 Physics Motivation</b> .....	<b>30</b>
<b>4.3 Run 13 pp2pp Request</b> .....	<b>32</b>
<b>5. Study of the Properties of QGP at RHIC Top Energy</b> .....	<b>34</b>
<b>5.1 Run 13 Request for Heavy Ion Physics</b> .....	<b>34</b>
<b>5.2 Run 14 Request for Heavy Ion Physics</b> .....	<b>38</b>
<b>5.3 Run 14 pp Reference Data Request</b> .....	<b>42</b>
<b>6. Study of the QCD Phase Diagram in <math>\sqrt{s_{NN}} \leq 20</math> GeV Au+Au Collisions</b> .....	<b>43</b>
<b>6.1 Goals and the Status of the Beam Energy Scan Phase-I (BES-I)</b> .....	<b>43</b>
<b>6.2 Selected Results from BES-I</b> .....	<b>45</b>
<b>6.3 BES-II Request</b> .....	<b>48</b>
<b>6.4 Proposal for STAR in Fixed-Target Mode</b> .....	<b>51</b>

RHIC Beam Use Request  
For Runs 13 and 14

*The STAR Collaboration*

May 28, 2012

## 1. Executive Summary

The STAR Collaboration makes the following two-year beam-use proposal, in order to achieve its spin and relativistic heavy ion physics goals on a timescale consistent with intense international interest and competition in these areas, as well as to utilize RHIC beams effectively, taking full advantage of planned improvements in machine and detector capability as a function of time:

Run	Energy	Time	System	Goal
13 <sup>(1)</sup>	$\sqrt{s} = 510 \text{ GeV}$	10 weeks	p+p	i) $W^{\pm} A_L: P^2 * \mathcal{L} = 50 \text{ pb}^{-1}$ ii) di-jets $A_{LL}: P^4 * \mathcal{L} = 15 \text{ pb}^{-1}$
		4 days	pp2pp	iii) $\sigma_{TOT}, A_N, A_{NN}, A_{SS}$ , Exclusive Central Production
	$\sqrt{s_{NN}} = 200 \text{ GeV}$	4 weeks	Au + Au	MTD e- $\mu$ correlation $2 \text{ nb}^{-1}$ (280M central events) HFT engineering run
14 <sup>(2)</sup>	$\sqrt{s_{NN}} = 200 \text{ GeV}$	10 weeks	Au+Au	HFT & MTD heavy flavor physics, $10 \text{ nb}^{-1}$ (500M M.B.) Fixed-target data taking <sup>(3)</sup>
	$\sqrt{s} = 200 \text{ GeV}$	5 weeks	p+p	i) Heavy ion reference data $\mathcal{L} = 40 \text{ pb}^{-1}$ (500M M.B.) ii) $\Delta(G)$ measurement $\mathcal{L} = 40 \text{ pb}^{-1}$ , 65% polarization

**Table 1.1:** STAR Beam Use Request for Runs 13 and 14.

(1) 20 cryo-week, 5 weeks for overhead and initial commissioning of two species. Total of 15 weeks production with two species.

(2) 20 cryo-week, 15 weeks production with two species.

(3) Fixed target data taking concurrently with the collider mode.

In this proposed physics-driven plan, the STAR Collaboration intends to make the most efficient use of RHIC beam time and upgrades in order to make timely progress in determining the polarizations of the light quark, anti-quarks by flavor, as well as the gluon helicity distributions of the proton, the collectivity and energy loss of the heavy flavors in high-energy nuclear collisions.

The primary goals of the proposed program are:

**Run 13:** 20 cryo-week, 15 weeks for physics production with two species. STAR's priorities for Run 13 are:

- a) Ten weeks:  $\sqrt{s} = 510$  GeV p+p collisions with the fully completed Forward GEM Tracker (FGT). These data will contribute to the measurements of  $A_L$  for W production at  $-2 < \eta < 2$  to determine the anti-quark polarizations and  $A_{LL}$  for di-jets to measure the shape of  $\Delta g(x)$ . 510 GeV p+p collisions to collect FOM =  $50 \text{ pb}^{-1}$  W physics data at both mid- and forward- rapidity and FOM =  $15 \text{ pb}^{-1}$  for gluon polarization,  $\Delta g(x)$ . A 55% or better polarization of the proton beams has been assumed in our estimation. This will be the initial physics production run after the complete installation of the FGT for the measurement of the parity violating single spin asymmetry,  $A_L$ , in W production at forward-rapidity.
- b) Four weeks:  $\sqrt{s_{NN}} = 200$  GeV Au+Au collisions with partially installed Muon Telescope Detector (MTD) ( $\geq 43\%$ ). The first e- $\mu$  correlation measurement will be made to explore the correlated charm contribution to dilepton measurements. In addition, this will be the engineering run for the newly constructed Heavy Flavor Tracker (HFT) detector, to test the new detector system in real collider environment in order to ensure the success of the physics run in Run 14.
- c) Four days: 510 GeV collisions with high  $\beta^* = 7.5\text{m}$  with transversely polarized beams, for studies of diffractive physics including spin dependence and coincident central particle production. This will yield the first data,  $\sigma_{TOT}$ , for example, at  $\sqrt{s} = 510$  GeV with the Roman Pots and a large dataset of Exclusive Central Production.

Note: The above are STAR Run 13 priorities. However, in order to maximize the efficiency in using the beam, we propose the order of the run plan as: c), a) and b).

**Run 14:** 20 cryo-week, 15 weeks for physics production with two species. Our priorities are:

- a) Ten weeks:  $\sqrt{s_{NN}} = 200$  GeV Au+Au collisions with both the HFT and the MTD. This is the first run in a multi-year program of precision measurements in the charm and bottom sector. The HFT will be used to directly reconstruct open charm hadrons, extracting the charm hadron collectivity and energy loss. The completed MTD will be used to measure quarkonium production in di-muon channels and extend e- $\mu$  correlations from Run 13. At the beginning of the run,

we will commission the Intermediate Silicon Tracker (IST) and Silicon Strip Detector (SSD) subsystems of the HFT. Further running will be needed in later years for measurements of the  $\mathcal{A}_C$ , and to extend the precision of the measurements of higher Upsilon states.

STAR will take fixed-target data to examine Au+Au collisions at  $\sqrt{s_{NN}} = 4.5$  GeV concurrently with the collider mode.

- b) Five weeks: 200 GeV polarized p+p collisions, corresponding to  $40\text{pb}^{-1}$  integrated luminosity and 65% polarization with the luminosity upgrade afforded by the electron lenses. The physics goals are to accumulate an initial heavy ion reference data sample with the HFT and MTD, and to provide significant further constrain on  $\Delta g(x)$  at large  $x$ . We estimate that this dataset will provide approximately 1/4 of the required luminosity and event count for precision heavy flavor measurements at STAR. Further running will be needed for precision measurements.

**BES-II Program**: The STAR Decadal Plan discussed the possibility that electron cooling might be required to enable high precision studies of the most interesting regions identified during Phase-I of the RHIC Beam Energy Scan (BES-I). Based on the BES-I results we conclude that the study of the QCD phase diagram requires substantially higher statistics of data for Au+Au collisions at  $\sqrt{s_{NN}} \leq 20$  GeV, corresponding to  $\mu_B \geq 200$  MeV. According to the simulations, electron cooling is necessary in order to reach the required luminosity at the proposed energy region. We therefore request that CA-D starts the e-cooling project.

## 2. Report on Run 12 Performance

### 2.1 Introduction

During Run 12, we have collected data for (i) 200 GeV transversely polarized p+p collisions. (ii) 510 GeV longitudinally polarized p+p collisions with the STAR newly installed FGT. (14 out of 24 quadrants were installed for the run.) (iii)  $\sqrt{s_{NN}} = 193$  GeV U+U collisions. (iv) As we prepare for the Beam User Request, we are collecting data for Cu+Au collisions at  $\sqrt{s_{NN}} = 200$  GeV.

From improvements to the STAR DAQ system and RCF capacity to analyze the data collected, STAR has to date collected a large dataset of approximately 1.5 petabytes in Run 12, to date increasing our overall dataset by 50% relative to all previous datasets combined, as shown in Figure 2.1.

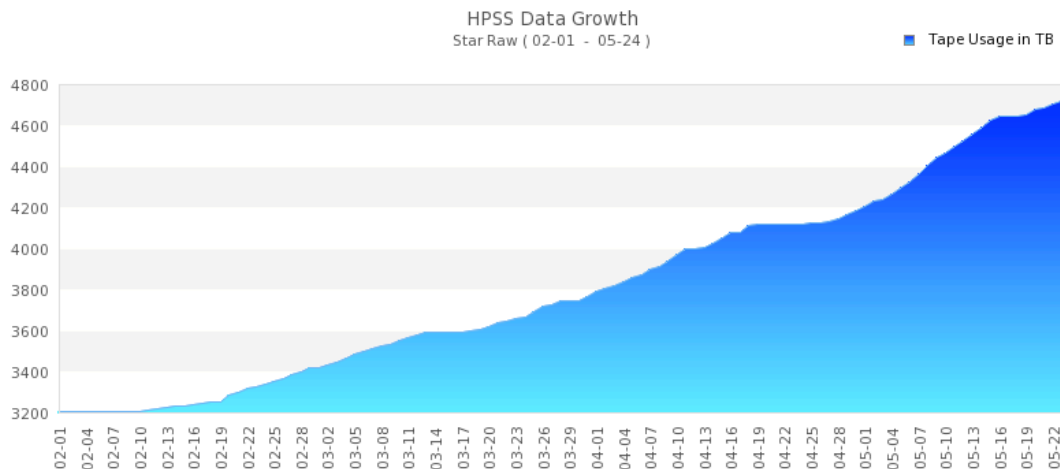


**Figure 2.1:** Integrated raw dataset size of STAR data, in Terabytes, over all years of STAR data taking. The plot begins at a baseline at the beginning of Run 12 and continues to May 25, partway through the Cu+Au run.

A detailed summary of the STAR performance during the Run 12 polarized proton running periods is given in Sect. 3.3.

### 2.2 Run 12 U+U Collisions

In the Beam Use Request from STAR last year, we requested a sample of 200M 0-10% central  $\sqrt{s_{NN}} = 193$  GeV U+U collisions, in order to study sufficient samples of body-body and tip-tip collisions by selecting a number of multiplicity bins in the top 1% central sample of events as selected by the Zero Degree Calorimeters, each bin having similar statistics to the overall statistics of RHIC Run 2. At the time, we estimated this would take 6 weeks, given historical STAR efficiency to sample the luminosity delivered by C-AD, STAR and C-AD uptime, and C-AD's ability to deliver luminosity in the first run using the EBIS source. Due to modifications of STAR procedures and improvements to our DAQ system to increase our sampling efficiency to an average of

80%, and more importantly due to the excellent performance of RHIC and especially the full stochastic cooling system, in Run 12 we collected this sample of events in less than 3 weeks. For reasons of bandwidth balance we collected it as a sample of 20M 0-1% central triggers, tagged within 100M 0-5% central triggers. A subsample of these 0-1% triggers, selected to be clean from pileup, were sent to a different data stream for rapid analysis.

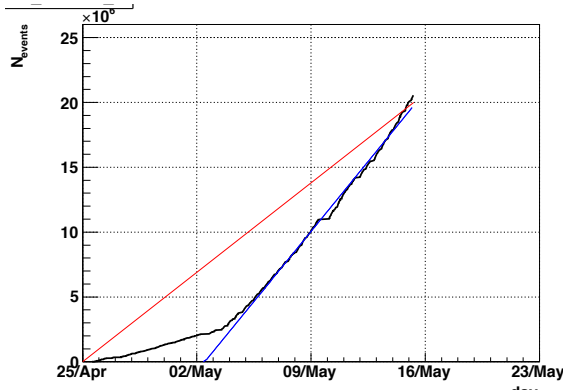


**Figure 2.2a** Number of top 1% U+U events as a function of days. In Run 12, STAR has collected about  $21 \times 10^6$  and  $350 \times 10^6$  events for central (top 1%) and minimum biased U+U collisions, respectively.

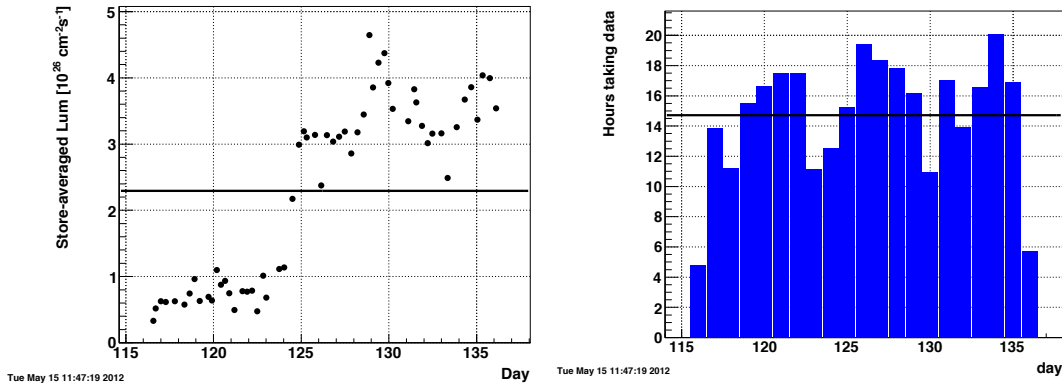


**Figure 2.2b:** Left: Store-averaged instantaneous luminosity sampled by STAR during the U+U running. Right: Number of hours per day during which STAR was taking data.

Figure 2.2a shows the time history of the number of events collected with a trigger selecting the 1% most central U+U collisions with the ZDCs, run at prescale 1, and so sampling all the luminosity delivered while STAR was running and live. The inflection point on 4 May is due to successful use of stochastic cooling, which increased the instantaneous luminosity averaged over a fill by a factor of 5, as shown in Figure 2.2b. Combined uptime of STAR and RHIC was extremely good, leading to an average of 15 hours of data taking per day, far above the historical average, allowing us to collect 350M (prescaled) minimum bias events rather than the sample of 200M minimum bias events proposed for a 6-week run in last year's BUR. Improvements to STAR's DAQ

allowed us to routinely collect data at greater than 800 MB/sec at deadtimes of a few percent, leading to an overall dataset of  $>0.5$  petabytes in less than three weeks.

In summary, the short U+U run in Run 12 was a great success, in which we reached or exceeded the goals laid out in the previous year's BUR, in half the time requested. The dataset will be of sufficient size to allow us to study the effects of body-body vs. tip-tip geometry on flow, along with a first look at the effect on partonic energy loss, and will provide a unique test if the previously observed charge-dependent azimuthal correlation signal originates from Chiral Magnetic Effect or more mundane background processes.

## 2.3 The FGT Performance

The commissioning of the Forward GEM Tracker (FGT) was a high priority goal during both the  $\sqrt{s} = 200$  and 510 GeV proton running in Run 12. The FGT is designed to extend STAR's charged-particle tracking capabilities to forward angles, which will allow measurements of the single-spin asymmetry  $A_L$  for leptonic W decay at both large positive and large negative electron and positron rapidities. The FGT may also allow for sensitive measurements of  $A_{LL}$  in the production of jets and dijets, and should serve as an effective charged particle veto for studies of inclusive photon and photon-jet spin asymmetries in which the photon is detected in the EEMC.

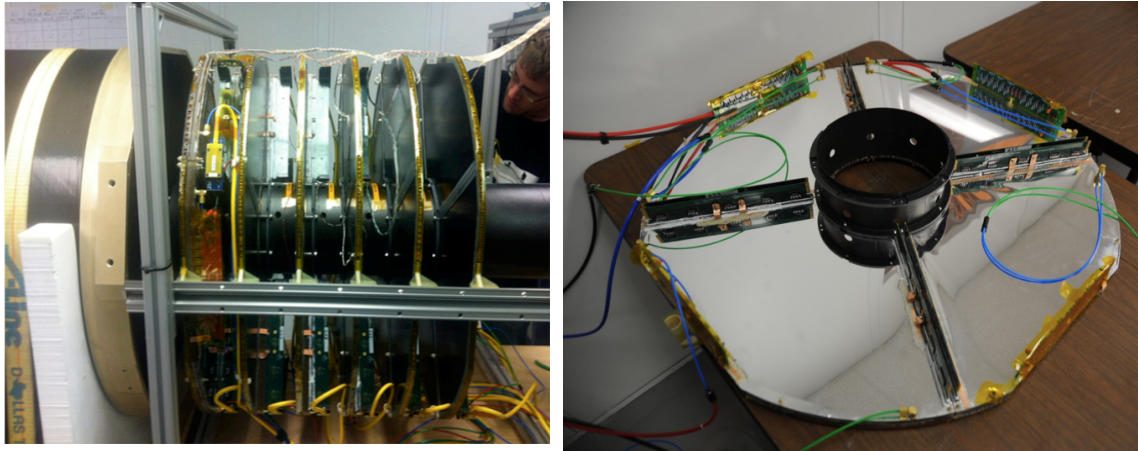


**Figure 2.3** (Left) Six FGT disks rest on an assembly fixture before insertion into the WSC. (Right) A single disk, composed of four quadrants of individual triple-GEM detectors.

The FGT and the west carbon fiber support cylinders (WSC) were installed in the fall of 2011. The complete FGT will hold six disks of triple-GEM detectors, in which each disk is divided into four quadrants. Each quadrant contains a 2D readout foil, with strips for both the radial (R) and azimuthal ( $\varphi$ ) readout directions. For Run 12, only the first disk (closest to the IR) was fully installed. Disks 2-6 were outfitted with two quadrants (A, B) for each disk. While the RHIC accelerator was cooling down and preparing for physics running, the FGT control GUI's were tested, the pedestals were determined and adjusted, an initial high voltage ramp was completed, and the gas

changed from a 70/30 to a 90/10 Ar/C02 mixture. During the 200 GeV pp running period, collisions were used to time-in the detector, optimize APV chip parameters, verify the location of the quadrants and APV chip channels on the physical detector, and perform a series of high voltage scans. Photographs of the FGT disk assembly, prior to insertion into the WSC and STAR, and a single disk showing the quadrant structure, are presented in Fig. 2.3.

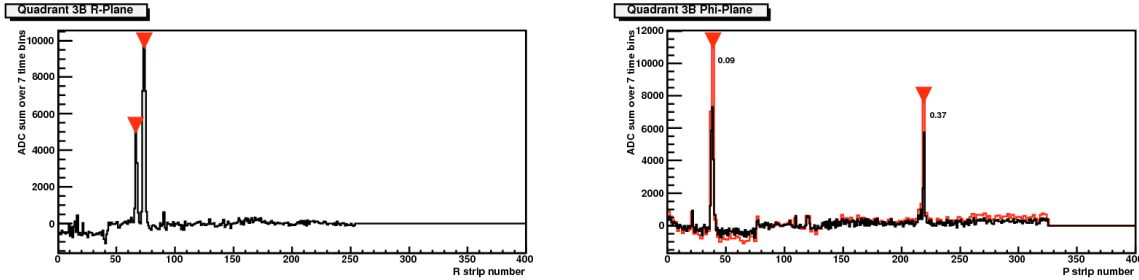


**Figure 2.4** Clusters found in the R and  $\phi$  planes in quadrant 3B using the “sum 3” cluster finding technique.

A minimum bias and EEMC high-tower trigger were used to collect FGT data during the 200 and 510 GeV running. A suite of offline software was used to process the data from these triggers, with the aim of characterizing signal pulses, finding and matching clusters from the R and  $\phi$  planes, and applying a helix tracking algorithm. Figure 2.4 shows the clusters found in a typical event in disk 3 quadrant B. Here, clusters are found by iterating over the strips in a single plane and summing the ADC values for three consecutive strips. The summed ADC value is represented on the y axis and the mean location of the three strip cluster on the x axis. All clusters with a summed ADC value greater than 1000 are kept for further analysis.

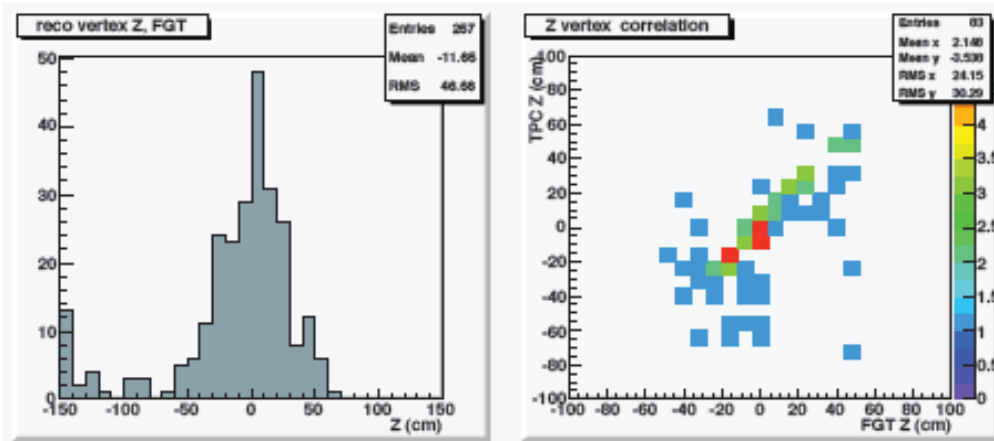


**Figure 2.5** The left panels contains tracks reconstructed from only FGT clusters for minimum bias triggers in run 13066101. The right panel shows the correlation between the FGT-only and TPC-only reconstructed z vertices.

If an event contains at least one R plane and one  $\phi$  plane cluster on at least 3 of the 6 disks, then these clusters are fed into a helix tracker. The tracker uses the beam line constraint in the transverse direction (*i.e.*, the position in x and y where the two proton

beams collide, as determined by the TPC), and the location on the disks that are closest and furthest from the interaction region, to constrain the fit. A track is labeled as “good” if the fit has  $\chi^2/\text{ndf} < 4$  and  $|Z_{\text{ver}}| < 50$  cm. Figure 2.5 shows the reconstructed  $z$  vertex using only FGT tracks, and demonstrates the strong correlation between the FGT-only and TPC-only vertices.

An important test of the FGT performance is to extract the track residuals in each quadrant. For example: If information from quadrant 3B is excluded from the track fitting procedure, and then all possible pairs of R- $\phi$  clusters in quadrant 3B are constructed, then the residual distribution – the distance – between the location of a good track pointing through quadrant 3B and the closest cluster should be highly peaked. The residuals in each plane of quadrant 3B for cluster pairs that fall within one cm of a good track are shown in the left and middle panels of figure 2.6. The summed ADC’s for the R- $\phi$  track matched clusters show a strong positive correlation (right panel in Fig. 2.6), indicating reasonable charge matching exists between the two planes.

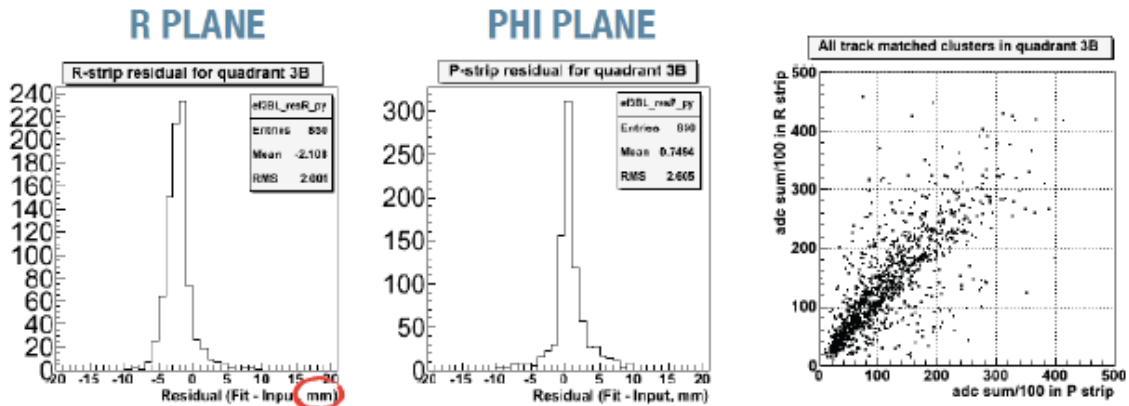


**Figure 2.6** Residuals for clusters in the R (left) and  $\phi$  (middle) planes of FGT quadrant 3B. Correlation (right) of summed ADC values for matched R-  $\phi$  clusters with residuals  $< 1$  cm.

Tracks that exclude clusters from quadrant 3B may also be used to give a first look at the quadrant efficiency. Figure 2.7 shows the uniformity of the efficiency (left) and relative error (right) for 3B. The extracted efficiency does not account for noise or dead areas in the detector, such as spacer supports, detector edges and dead channels. Reasonable uniformity has been found in both cases. Note that the data used in this analysis comes from statistically limited high voltage scan runs. Since track multiplicity increases with rapidity, the white regions at the outer radius of disk simply reflect the inverse correlation between track reconstruction and rapidity. The refinement of the efficiency and residual analysis is an ongoing effort and will also be a major focus of further HV and gas mixture studies during the ongoing Cu-Au running using a dedicated low-multiplicity rigger.

The components for 14 additional triple-GEM detectors needed to complete the FGT (including four for spares) have been ordered. They will be tested, assembled onto frames, and mounted inside the existing FGT structure during the 2012 summer

shutdown. The FGT is on schedule to be completed and installed in STAR for run 2013.

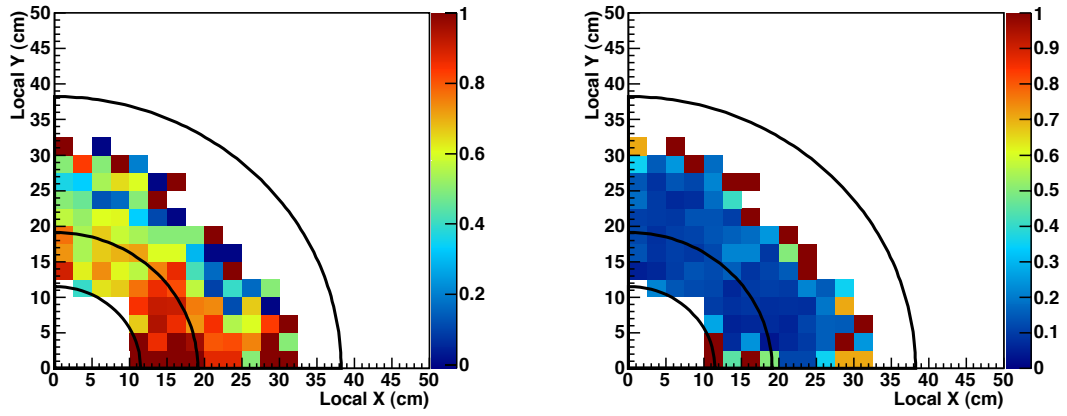


**Figure 2.7** The efficiency (left) and relative error (right) for FGT quarter section 3B.

### 3. Study of the p+p Collisions

#### 3.1 Overview

The STAR spin physics program seeks to advance our understanding of the spin and flavor structure of the proton in terms of its constituent quarks and gluons, exploiting the unique capability of RHIC to provide access to polarized pp collisions. Using longitudinally polarized beams, one can probe the helicity preferences of the gluons and (flavor-separated) antiquarks, to determine the contribution of each to the total spin of the proton. With spins transverse to their momentum direction, the pp collisions exhibit kinematic and dynamical effects that are directly sensitive to quark transversity and partonic motion within the proton, e.g., orbital angular momentum. This program is complemented by studies of polarized pp elastic scattering and central exclusive production, in which a far-forward proton is detected intact.

RHIC has just completed a very successful  $pp$  run as part of Run 12, in which STAR collected a transversely polarized data sample with single-spin figure-of-merit  $\text{FOM}_{\text{SS}} \equiv P^2L \sim 7.7 \text{ pb}^{-1}$  at  $\sqrt{s} = 200 \text{ GeV}$ , and a longitudinal data set of  $\text{FOM}_{\text{SS}} \sim 25 \text{ pb}^{-1}$  at  $\sqrt{s} = 510 \text{ GeV}$ . Each of these required about 4-5 weeks of running, and represents a significant increase in the rate at which high-quality  $pp$  data can be acquired at RHIC. Additionally, the beam polarizations attained at 510 GeV were marked higher than those in Run 9. More detail on both RHIC and STAR performance in Run 12, and a brief look at the quality of results that can be expected, are provided in section 3.3 below.

To build on these successes we request 10 weeks of polarized  $pp$  operation at  $\sqrt{s} = 510 \text{ GeV}$  in Run 13. Essentially all of the data would be taken with beams longitudinally polarized at STAR. If we conservatively estimate that the sampled luminosity and polarization would be similar to that demonstrated in Run 12, this would allow us to collect an additional  $160 \text{ pb}^{-1}$  of longitudinal data, for a  $\text{FOM}_{\text{SS}}$  of  $\sim 75 \text{ pb}^{-1}$  at  $\sqrt{s} = 510 \text{ GeV}$  for Runs 12 and 13 combined. Such a data set would significantly advance the STAR spin physics effort; in particular, our analyses would focus on:

- Extraction of the parity-violating single-spin asymmetry  $A_L$  in  $W^\pm$  production at mid-rapidity. Using the STAR TPC and Barrel EMC to identify isolated, high- $p_T$  lepton ( $e^\pm$ ) candidates in events with little ‘away-side’ energy, one would achieve a factor of about 50 improvement in  $\text{FOM}_{\text{SS}}$  relative to the results published previously based on Run 9 data [1]. Beyond simply reducing error bars, this would allow the first detailed look at the  $\eta$  dependence of  $A_L$ , which is driven predominantly by the quark polarization at one extreme, but becomes sensitive to anti-quark polarizations at the other. A more in-depth discussion of these ideas, and realistic projections, are given in section 3.4.
- First measurements of  $A_L$  in  $W^\pm$  production at forward rapidities,  $1 < \eta < 2$ . Over the pseudo-rapidity range  $1 < \eta < 1.4$  one can extend our current analysis algorithms, but using the Endcap EMC to extract the lepton’s  $E_T$ , rather than the Barrel. Near  $\eta \sim 1.4$ , though, the TPC track reconstruction efficiency is falling

rapidly, and we will rely on information from the new Forward Gem Tracker (FGT) to: (1) ensure that there is a high- $p_T$  track pointing towards the Endcap tower of highest  $E_T$ ; and (2) determine the charge sign of this track. For this latter task, we will need to combine points from the TPC (to identify the event vertex), the FGT (most of the track), and the Endcap EMC (a final point in the Shower Max Detector). A brief summary of the status of the FGT and its commissioning in Run 12 can be found in section 2.3.

- Increased precision in measurements of the double-spin asymmetry  $A_{LL}$  in coincident di-jet production. The quality of the data set projected for Runs 12 + 13 will be such that we can move beyond the “Bjorken- $x$  averaged” results for the gluon polarization that characterize all inclusive studies, and begin to truly map out the function  $\Delta g(x)$ . To fully exploit this capability, our algorithms for full jet reconstruction in the Endcap, currently under development, will need to become quite a bit more sophisticated. The extent to which FGT information may help is yet to be explored.

In addition to the above analyses, we will continue to examine our inclusive jet data, though in the low  $x_T$  region, which only becomes accessible at these higher collision energies, the quality of our results will be limited by systematic uncertainties (relative luminosities and trigger bias), rather than statistics. Other coincident channels, such as photon-jet events with a forward-going photon detected in the Endcap, will be statistics limited, but these can provide complementary information on  $\Delta g(x)$ , with less dependence on choice of a specific PDF parameterization, for example.

Finally, we note that while this projected data sample will yield important physics results, both greatly increasing the quality of our current analyses, such as di-jets, and providing a “first look” at new efforts, such as forward/backward  $W$ s, most of these programs continue to be statistics-limited, and we look forward to – and rely on – additional large  $pp$  data sets, at  $\sqrt{s} = 200$  and 500 GeV, that will be taken in future runs.

## 3.2 Recent Highlights from the STAR Spin Program

Since the last RHIC PAC, ongoing analyses of polarized  $pp$  data acquired in earlier runs have led to many new results, a few of which are highlighted here.

The inaugural run at  $\sqrt{s} = 500$  GeV in 2009 yielded a first measurement of the longitudinal single-spin asymmetry  $A_L$  in  $W^\pm$  production, followed by rapid publication of this essential milestone [1]. Extracting the cross sections for  $W^\pm$  and  $Z$  production in  $pp$  collisions took a while longer, though, due largely to uncertainties in the absolute luminosity determination at this higher energy. Our final results, published in [2], are presented in Fig. 3.1, along with the “world’s supply” of  $W$  and  $Z$  production data from all previous experiments that used either  $pp$  or  $ppbar$  collisions. It is only in the last couple of years that measurements have been carried out at  $pp$  colliders, where one is sensitive to the anti-quark distributions inside the nucleon; coincidentally, the first

results from the LHC and RHIC – the highest and lowest center of mass energies, respectively, on the plot – appeared within a few months of each other. The STAR cross sections for  $W^+$  ( $W^-$ ) production, indicated by the solid (open) blue circles, are seen to be in excellent agreement with theoretical predictions carried out at NLO with the FEWZ program [3] using the MSTW 2008 PDF set [4].

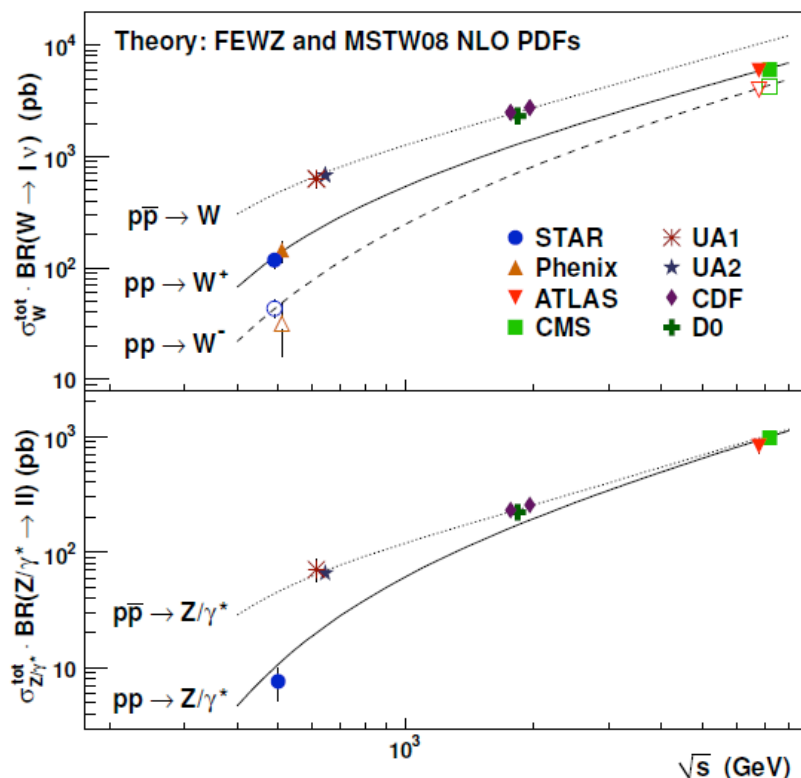


**Figure 3.1** Measurements of  $W$  and  $Z/\gamma^*$  ( $70 < m_{ee} < 110 \text{ GeV}/c^2$ ) total cross sections times branching ratio versus center-of-mass energy. These points exhaust the world’s supply of such measurements.

STAR also continues to make progress in understanding forward meson production, where for more than 20 years we have known that spin asymmetries for forward pion production, studied in collisions of transversely polarized protons, are large in magnitude and depend on the isospin projection of the produced mesons, *i.e.*, the analyzing power  $A_N$  is opposite in sign for  $\pi^+$  vs.  $\pi^-$  production. Though several extensions of the pQCD collinear framework have been proposed to explain these data, it is fair to say that our theoretical understanding remains in its early stages.

STAR has made several important contributions to this program, primarily through study of forward neutral pion production in  $pp$  collisions (see, for example, ref. [5]). This effort has recently been extended to include the first measurements at  $\sqrt{s} = 200 \text{ GeV}$  of the transverse spin asymmetry  $A_N$  for the  $\eta$  meson, a member of the pseudo-scalar octet that is also isospin  $I_3 = 0$ , like the  $\pi^0$ . STAR results for  $\pi^0$  as a function of  $x_F$  are presented in Fig. 3.2 for data taken at an average pseudo-rapidity of 3.68. These data can be compared to the values of  $A_N$  found for  $\pi^0$  production at the same pseudo-rapidity, and to an earlier analysis of the same data analyzed using slightly different

requirements [5]. The two sets of  $\pi^0$  results are seen to be consistent within their (correlated) errors, while the analyzing power for the  $\eta$  meson is roughly 2-2.5 times larger, especially for  $x_F > 0.5$ . This difference in  $A_N$  between the two mesons is particularly interesting, given their similar up and down quark content. The  $\eta$  is an isospin singlet state, and is predicted to have a larger strange quark component than the  $\pi^0$ , which in some models [6] leads to a sizable  $A_N$  via an initial-state twist-3 effect for only the strange quarks. Envisioned measurements of  $A_N$  for non-hadronic final states, such as prompt photons, may aid in understanding the mechanism for these large asymmetries.

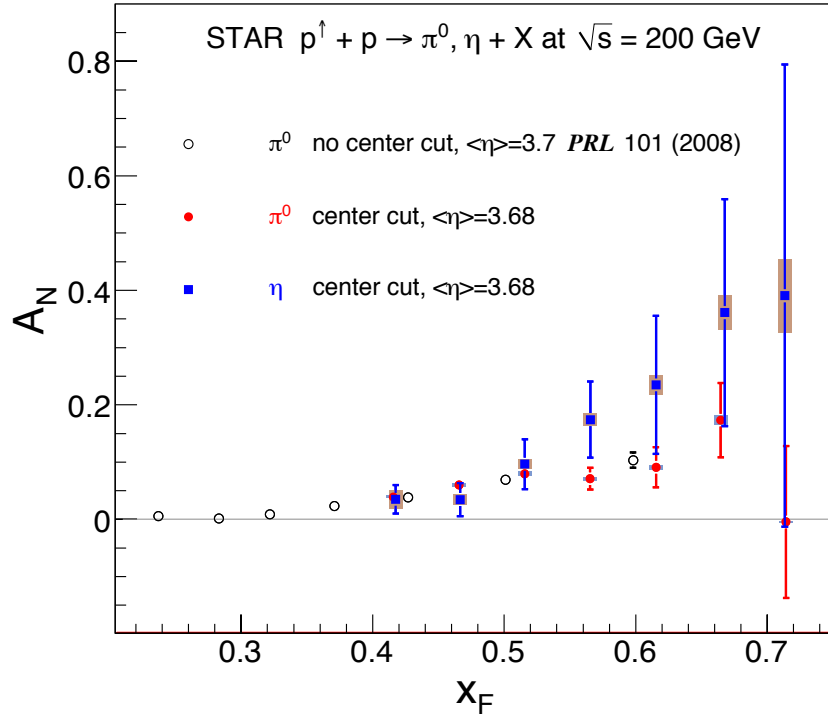


**Figure 3.2** Measured values of  $A_N$  as a function of  $x_F$  at an average pseudo-rapidity of 3.68 for  $\pi^0$  and  $\eta$  mesons at  $\sqrt{s} = 200$  GeV. The error bars represent statistical uncertainties only; the boxes show the systematic uncertainties.

Experimental studies using transversely polarized proton beams also provide a fairly direct probe of the quark transversity function  $h(x)$  which can be thought of as the probability of finding a transversely polarized quark of momentum fraction  $x$  in a transversely polarized proton. If one integrates over (or is not sensitive to) the intrinsic parton momentum, then to leading twist  $h(x)$ , together with the helicity and momentum distribution functions provides a complete description of the spin structure of the nucleon. Most spin observables, however, will vanish when averaged over the intrinsic (internal to the proton) momentum of the quarks due to angular momentum conservation, so a second vector must be detected in the final state.

These general arguments lead naturally to the study of di-hadron correlations within a jet, *i.e.*, at relatively small opening angle, where one works with the transverse

momentum  $p_T$  and the invariant mass  $M$  of the pair, rather than with individual particle  $p_T$ . Correlations can be described in terms of the product of the transversity  $h(x)$  and the so-called Interference Fragmentation Function, IFF, which is a chiral-odd quantity. Extracting the IFF in polarized  $pp$  collisions at high energy is of particular interest, in that this will constrain  $h(x)$  at higher values of  $x$  than competing measurements. With its broad acceptance for charged particles in the TPC, STAR is well positioned to carry out these measurements near mid-rapidity.

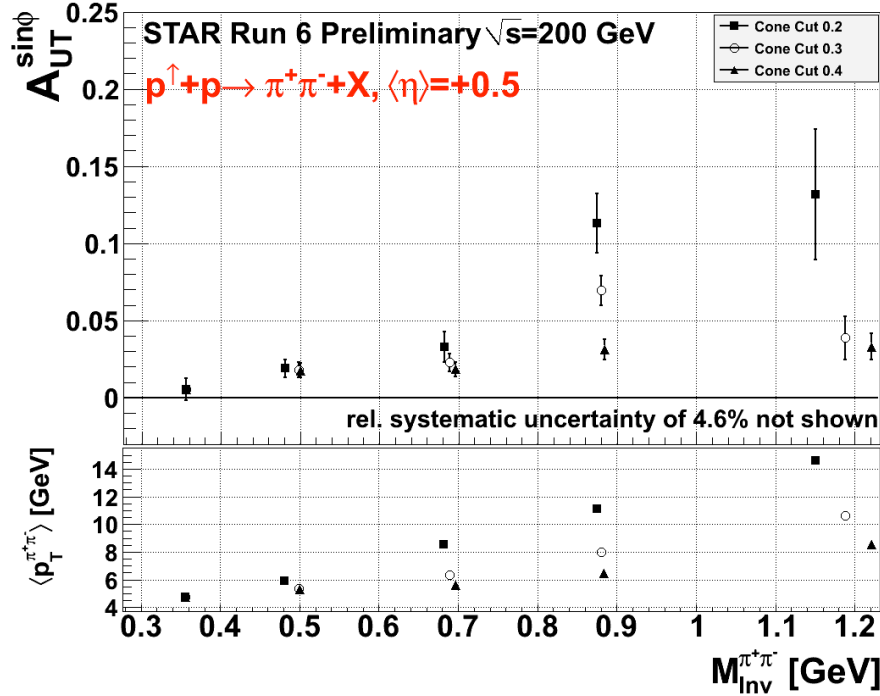


**Figure 3.3** (top) Preliminary measurements of the transverse single-spin asymmetry  $A_{UT}$ , as defined in the text, as a function of the invariant mass of the unlike-sign di-pion. The choice of cone cut radius is strongly correlated with the average transverse momentum of the pair, as can be seen in the kinematic plot (bottom).

STAR has recently completed a first analysis of the transverse single-spin asymmetry  $A_{UT}$ , which characterizes the azimuthal dependence of the correlated hadron pair on the spin of the parent quark. This function is determined by measuring the dependence of the hadron pair yield on the azimuthal angle  $\Phi_{RS}$  between the vector difference  $R$  of the momentum of the two hadrons and the nucleon spin direction  $S$ , that is:

$$A_{UT}^{\sin\Phi} = A_{UT} \sin(\Phi_R - \Phi_S) = \frac{\sigma^\uparrow - \sigma^\downarrow}{\sigma^\uparrow + \sigma^\downarrow} \sin(\Phi_R - \Phi_S).$$

Results are shown in Fig. 3.3 for this quantity as a function of the di-hadron invariant mass, where the hadron pair is required to be two charged pions of unlike sign. The opening angle range between the pair is varied, leading to large (weak) variations in  $p_T$  and  $M$  of the pair, as illustrated in the lower part of the figure. These data represent the first significantly non-zero transverse spin asymmetry measured at mid-rapidity at STAR, and should provide new insights into the fundamental transversity distribution function  $h(x)$ .

The second observable is of leading charged pions inside a reconstructed jet. In this case one is looking for correlations between the azimuthal distribution of the pion inside the jet and the spin orientation of the parent proton. Similarly to the IFF case, these correlations are sensitive to the product of transversity  $h(x)$  and the Collins Fragmentation Function  $\Delta D(z)$ , also a chiral odd quantity. Measurements in semi-inclusive deep inelastic and electron-positron scattering have shown  $\Delta D(z)$  to be sizable and increasing with increasing pion momentum fraction  $z$ .

The differential cross-section for this process can be written in terms of the unpolarized cross-section and a sine weighted moment associated with the Collins function:  $d\sigma = d\sigma_{\text{unpol}}(1 + A_N \sin(\varphi_h - \varphi_S))$ . Here  $\varphi_S$  is the angle of the polarized proton spin direction with respect to the reaction plane formed by the reconstructed jet and the beam axis.  $\varphi_h$  is the angle between the transverse momentum vector of the charged pion with respect to the jet axis and the reaction plane and  $A_N$  is related to  $h(x)$  and  $\Delta D(z)$ .

Figure 3.4 shows a recent measurement of this Collins asymmetry  $A_N$  made using mid-rapidity jets reconstructed at STAR. It was calculated by forming the ratio of the sum of the  $\sin(\varphi_h - \varphi_S)$  weighted events and the sum of the polarization  $P$  weighted events. Systematic errors were conservatively estimated to be  $\pm 0.023$  for the  $\pi^+$  and  $\pi^-$  results independently.

Both the IFF and Collins analysis were exploratory measurements made using Run 6 transverse data. Indications of non-zero asymmetries motivated the extended 200 GeV running during Run 12. The expected sensitivities for these observables are discussed in the following section.

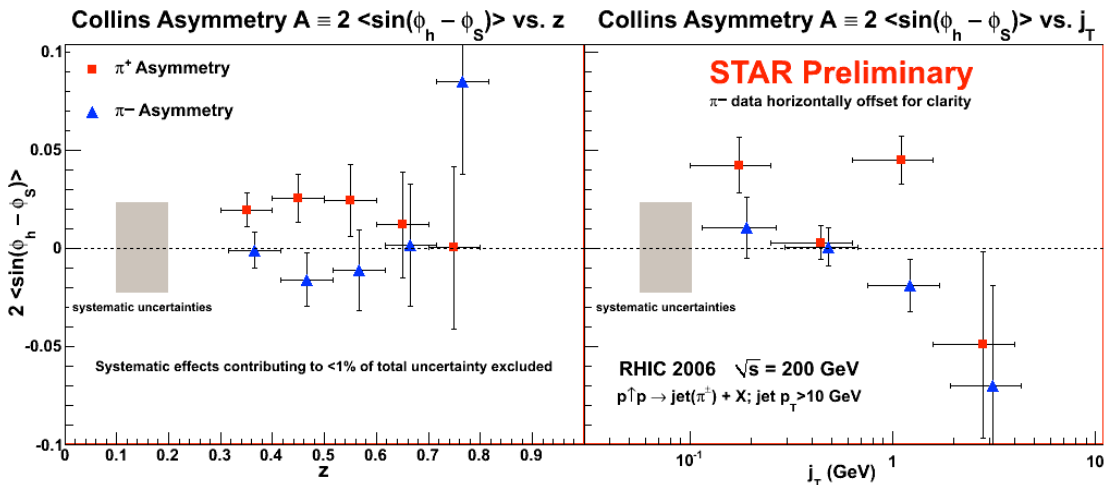


**Figure 3.4** Preliminary results of the Collins moment for leading  $\pi^+$ (red) and  $\pi^-$ (blue) particles within mid-rapidity jets reconstructed by the STAR detector. Statistical errors are shown on data points and the grey shaded band indicates the systematic error bar for  $\pi^+$  and  $\pi^-$  separately.

### 3.3 Summary of Run 12 Polarized Proton Collisions

Polarized proton beams were collided at both  $\sqrt{s} = 200$  and  $\sqrt{s} = 510$  GeV center-of-mass energies in run 12. The proton spins were oriented transversely during the four-week 200 GeV period, and longitudinally during the 4.5 weeks of 510 GeV running. The luminosity and polarization goals were based on the projected RHIC performance from the BNL CAD ([www.rhichome.bnl.gov/RHIC/Runs/RhicProjections.pdf](http://www.rhichome.bnl.gov/RHIC/Runs/RhicProjections.pdf)) for run 12, and assume a STAR sampling efficiency of 60%. The accelerator performed extremely well during the 2012 run, delivering integrated luminosities near the maximum of the projected range, and meeting polarization goals of 60% (55%) in 200 (510) GeV. Figure 3.5 contains plots of the yellow and blue beam polarization, as measured by the hydrogen jet target, versus fill for the 200 (left) and 510 (right) GeV periods.

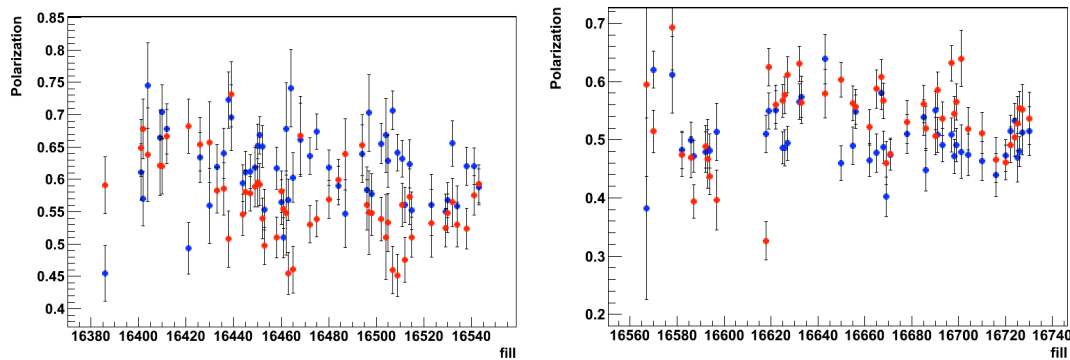


**Figure 3.5** Blue and yellow beam polarization versus fill number, as measured by the hydrogen jet target, for the transverse (left) and longitudinal (right) running period.

**Physics results:** The STAR Run 12 beam use proposal requested 10 weeks of transverse running to collect a data set with figure of merit (FOM)  $P^2L = 7.2 \text{ pb}^{-1}$ . Exceptional accelerator performance and high sampling rates at STAR during the 2012 run resulted in a sampled FOM of  $\sim 7.74 \text{ pb}^{-1}$  in less than half the requested running time. Preliminary measurements of the Interference Fragmentation Function and Collins results from  $\sim 2.2 \text{ pb}^{-1}$  of transverse data taken in 2006 (see section 3.2) indicate that STAR is seeing non-zero asymmetries, which are sensitive to quark transversity distributions, at mid-rapidity. Data collected in Run 12 will allow these asymmetries to be measured with higher precision and increased kinematic coverage; see Fig. 3.6 for quantitative projections. These data will also be used to provide tight constraints on the mid-rapidity inclusive jet  $A_N$ , which may be sensitive to the gluon Sivers contribution. At forward rapidities, the 2012 data will permit study of the  $x_F$  dependence of inclusive  $\pi^0$  and  $\eta$  meson production, as well as make a first measurement of the inclusive photon  $A_N$ , in the forward meson detector (FMS) at STAR.

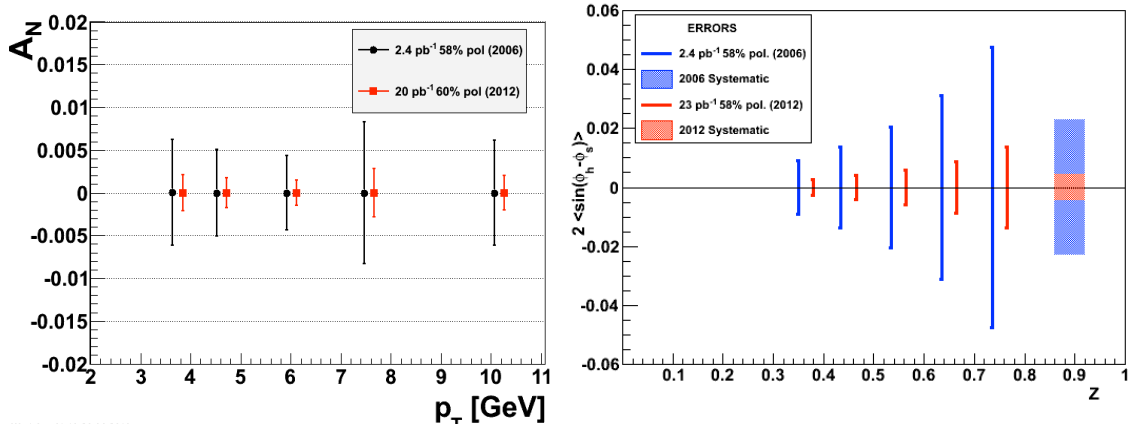


**Figure 3.6** Run 6 errors compared to Run 12 projections for the mid-rapidity Interference Fragmentation Function (left) and Collins (right) asymmetries.

The total FOM for the  $\sqrt{s} = 500$  GeV longitudinal running period was significantly higher in Run 12 compared to the performance in Runs 9 and 11. STAR collected a dataset with FOMs of  $P^2L = \sim 25 \text{ pb}^{-1}$  for the W single-spin analysis, and  $P^4L = 7.5$  for the double-spin ( $A_{LL}$ ) jet, hadron, and photon measurements. This is nearly a factor of four improvement in FOM rate compared to what was achieved in Run 11 ( $\sim 3 \text{ pb}^{-1}$  in two weeks of running). In Fig. 3.7 we show the statistical precision and kinematic reach expected for the inclusive jet  $A_{LL}$  results from the 2012 data set.

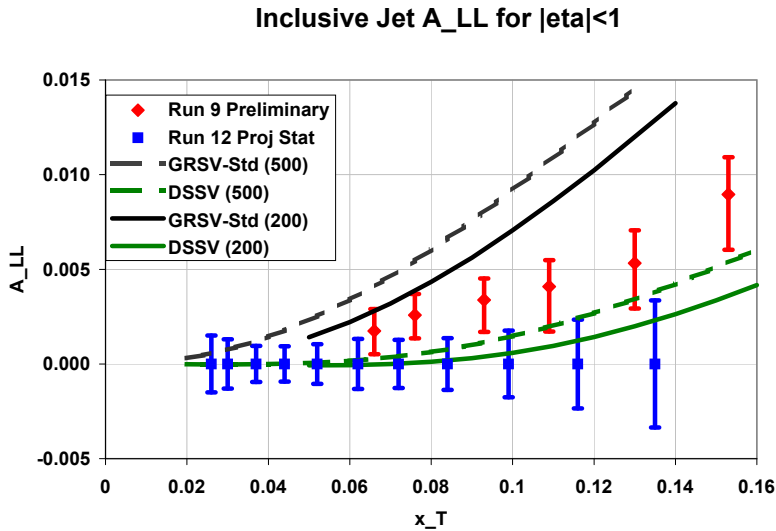


**Figure 3.7** Inclusive jet sensitivity from the run 12 510 GeV data compared to the run 9 preliminary result.

A fast offline analysis of the  $W^+$ ,  $W^-$ , and Z signal was performed, using only about 1/4 of the total 510 GeV dataset, or close to  $\sim 20 \text{ pb}^{-1}$ . The top left panel in figure 3.8 shows the charge separated track  $1/p_T$  for leptons with  $|\eta| < 1$  as measured by the TPC, versus the transverse energy ( $E_T$ ) determined by the barrel calorimeter (BEMC). The band observed in the upper (lower) half of the plot originates from  $W^+$  ( $W^-$ ) decay. The top right plot shows the Jacobian peak of the  $e^+e^-$  daughters from W candidates in the

BEMC. A rough cut at  $E_T > 20$  GeV results in a total  $W$  yield of 668 events. The lower left panel shows the equivalent Jacobian peak for  $W$  candidates reconstructed from tracks with  $1.0 < \eta < 1.4$  in the TPC and where  $E_T$  is thus measured in the endcap calorimeter (EEMC). A statistically limited, but clean sample, of  $Z$  bosons was reconstructed using unlike charge pairs where each of the back-to-back leptons satisfied the  $W$ -decay lepton isolation cuts. The invariant mass distribution is shown in the lower right panel of Fig. 3.8, and exhibits a clear peak at the expected mass. Note that this also provides a very high-energy check on the average BEMC tower gain calibration.

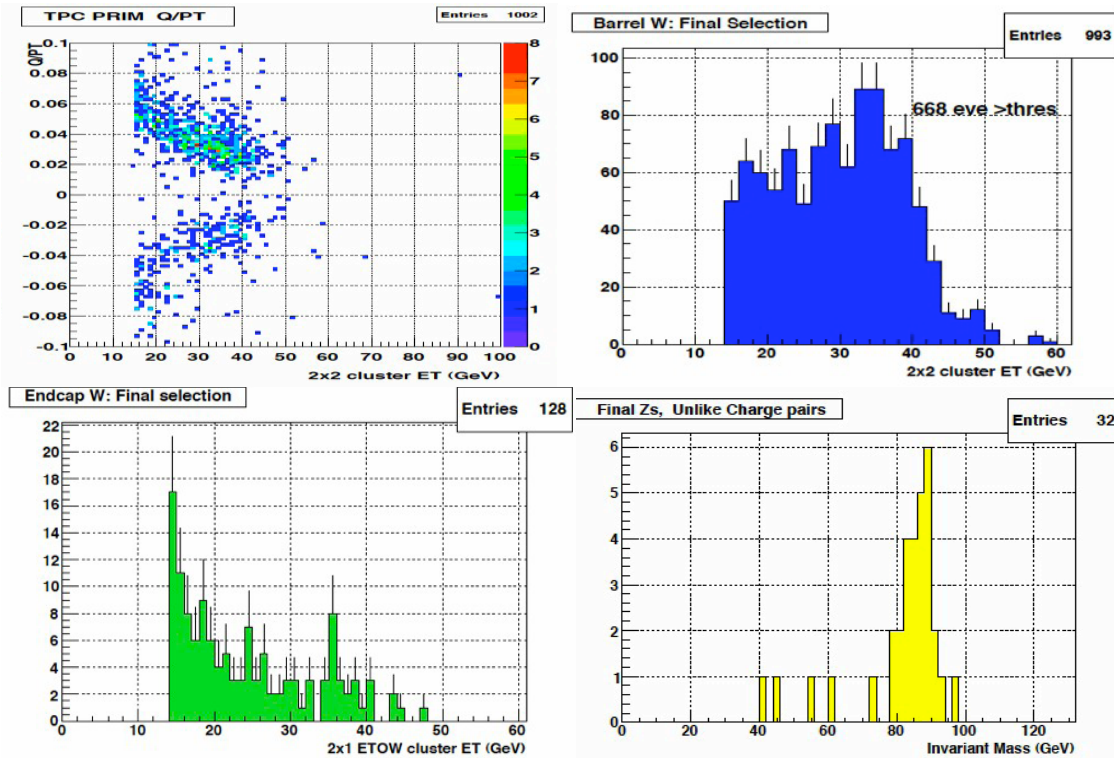


**Figure 3.8** The charge-sign separated  $Q/p_T$  vs. BEMC ET for midrapidity tracks (top left). Any track originating from a good vertex and with  $p_T > 10$  GeV is considered an  $e^+/e^-$  candidate. The Jacobian peak for  $W$  candidates in the BEMC (EEMC) is shown in the top right (bottom left) panel. Unlike sign charge pairs are used to reconstruct  $Z$  candidates in the BEMC (bottom right).

### 3.4 Run 13 Request for 500 GeV $pp$ Collisions

The recently completed 5-week  $\sqrt{s} = 510$  GeV period of Run 12 provided the first high-statistics data set for STAR to explore the separated quark and anti-quark polarizations in the proton with measurements of  $A_L$  for  $W$  production. It also provided the first high-statistics opportunity for STAR to measure  $A_{LL}$  for jet and di-jet production at  $\sqrt{s} = 510$  GeV, thereby extending our studies of the gluon polarization in the proton to lower  $x$ . During the run, STAR sampled  $82 \text{ pb}^{-1}$  with the  $W$  and high- $p_T$  jet patch triggers. Preliminary reports from the polarimetry group indicate that the beam polarization

averaged approximately 55% (after corrections are applied to the on-line values to account for the polarization profile). The FOM was  $P^2L = 25 \text{ pb}^{-1}$  for  $A_L$  and  $P^4L = 7.5 \text{ pb}^{-1}$  for  $A_{LL}$ .

Both  $A_L$  for  $W$  production and  $A_{LL}$  for di-jet production are luminosity-hungry measurements that have long been recognized to be multi-year efforts. During Run 13, STAR proposes to devote 10 physics weeks to longitudinally polarized  $pp$  collisions at  $\sqrt{s} = 510 \text{ GeV}$  in order to build on the success of Run 12. Conservatively, we assume this will allow us to sample twice the FOM that we recorded during Run 12. The STAR FGT will also be complete for Run 13. Thus, the run will both significantly increase the precision of the STAR  $W A_L$  and di-jet  $A_{LL}$  measurements and extend the kinematic reach of the  $W A_L$  measurement to  $|\eta| < 2$ .

Polarized inclusive deep-inelastic scattering (DIS) measurements have determined the polarizations of the up quarks+anti-quarks,  $\Delta u + \Delta \bar{u}$ , and down quarks+anti-quarks,  $\Delta d + \Delta \bar{d}$ , with high precision. The separate quark and anti-quark polarizations,  $\Delta u$ ,  $\Delta \bar{u}$ ,  $\Delta d$ , and  $\Delta \bar{d}$ , have been inferred from semi-inclusive DIS experiments, but the uncertainties remain large. A detailed understanding of the anti-quark polarizations will elucidate the origin of the anti-quark sea in the nucleon and the role that the sea plays in nucleon structure. For example, the nucleon sea is known to be flavor asymmetric, with  $\bar{d} > \bar{u}$  over a broad  $x$  range [8]. Several models of the nucleon structure, including meson cloud and chiral quark soliton models, predict that  $\Delta \bar{u} - \Delta \bar{d}$  should be of the same order as  $\bar{d} - \bar{u}$ . Recent global analyses of the polarized parton distribution functions are qualitatively consistent with this expectation, but the uncertainties remain too large to draw clear conclusions [9]. New, high precision measurements are essential to address these questions.

The parity-violating longitudinal single-spin asymmetry,  $A_L$ , for  $W$  production in polarized  $pp$  collisions is an ideal tool to separate the polarizations of the quarks and anti-quarks.  $W$  bosons are produced in  $pp$  collisions via the weak interactions  $u + \bar{d} \rightarrow W^+$  and  $d + \bar{u} \rightarrow W^-$ . The weak interaction violates parity maximally, with only left-handed quarks and right-handed anti-quarks participating in these reactions. Thus,  $W$  production is an excellent means to determine the polarizations of the quarks and anti-quarks within the interacting protons. The nuclear physics community has recognized the importance of  $W$  longitudinal asymmetry measurements, which are called for in DOE performance milestone HP8.

STAR performed its first proof-of-principle  $W$  asymmetry measurement during Run 9 [10].  $W$ 's were observed at mid-rapidity through their leptonic decays  $W^\pm \rightarrow e^\pm + \nu$ . The FOM available during Run 9 was only sufficient to determine the asymmetry in a single pseudorapidity bin, spanning  $|\eta| < 1$ , as shown in Fig. 3.9. The polarizations of the individual quark and anti-quark flavors can be separated by observing the  $\eta$ -dependence of the asymmetries of the decay  $e^\pm$ . As discussed in the Run 12 summary above, the FOM obtained during Run 12 is now sufficient to permit us to begin investigating the  $\eta$  dependence, but substantially more statistics are needed for precision separations of the quark and anti-quark polarizations. Run 13 will be a major

step along this path. Figure 3.10 shows the precision that STAR will achieve for  $A_L$  vs.  $\eta$  when the results from Runs 12 and 13 are combined together, compared to the current uncertainty from the DSSV global analysis. For the first time, the combination of Runs 12 and 13 will permit STAR to achieve statistical uncertainties comparable to the entire current world knowledge for several individual bins at mid-rapidity. These results should lead to a reduction in the uncertainties of the separate quark and anti-quark polarizations by a factor of  $\sim 2$  in the region  $x \gtrsim 0.1$ .

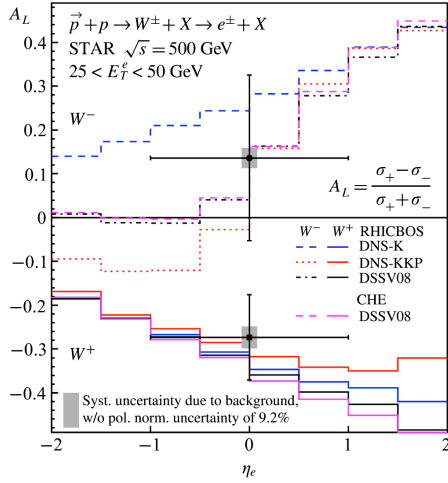


**Figure 3.9** STAR measurements of  $A_L$  for  $W^\pm \rightarrow e^\pm + \nu$  from Run 9 [10].

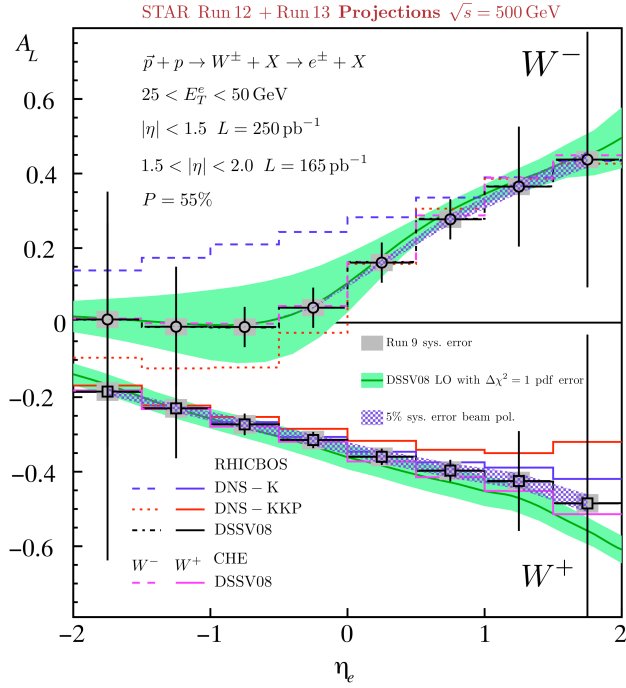


**Figure 3.10** Projected precision of STAR measurements of  $A_L$  for  $W^\pm \rightarrow e^\pm + \nu$  production. The green bands show the  $\chi^2+1$  uncertainty ranges from the DSSV global analysis [8]. The points with  $|\eta| < 1.5$  assume the combined Runs 12+13 FOM. The points at  $1.5 < |\eta| < 2$ , which require the complete STAR FGT, assume only the Run 13 FOM.

Determining the gluon polarization in the nucleon,  $\Delta g$ , has also been a long-term RHIC goal. The virtual photons in DIS and semi-inclusive DIS only couple to the quarks and anti-quarks in the nucleon, not the gluons. Thus, polarized DIS measurements are only sensitive to  $\Delta g$  indirectly, via  $Q^2$  evolution. The  $Q^2$  range that has been explored in polarized DIS experiments is rather small, making the uncertainties in  $\Delta g$  from DIS and semi-inclusive DIS large. In contrast, at leading order in pQCD polarized  $pp$  collisions at RHIC mostly involve quark-gluon and gluon-gluon scattering. The partonic asymmetries,  $\hat{a}_{LL}$ , for  $qg$  and  $gg$  scattering are large, so jet and hadron production at RHIC are excellent probes of the gluon polarization. The nuclear physics community

has recognized the importance of these measurements. DOE performance milestone HP12 calls for measurements “to determine if gluons have appreciable polarization over any range of momentum fraction between 1 and 30% of the momentum of a polarized proton.”

The DSSV polarized parton distribution fit [8] provides a framework in which to address this question. DSSV is the first global analysis to include DIS, semi-inclusive DIS, and RHIC data on an equal footing. de Florian *et al.* found that the RHIC data that had been obtained through Run 6, inclusive  $\pi^0 A_{LL}$  measurements from PHENIX and inclusive jet  $A_{LL}$  measurements from STAR, provided the dominant constraints on the gluon polarization, even though they only represented <10% of the data points included in the global analysis. DSSV concluded that the gluon polarization is “small” in the range  $0.05 < x < 0.2$ , which is primarily sampled by  $\sqrt{s} = 200$  GeV  $pp$  collisions at RHIC.

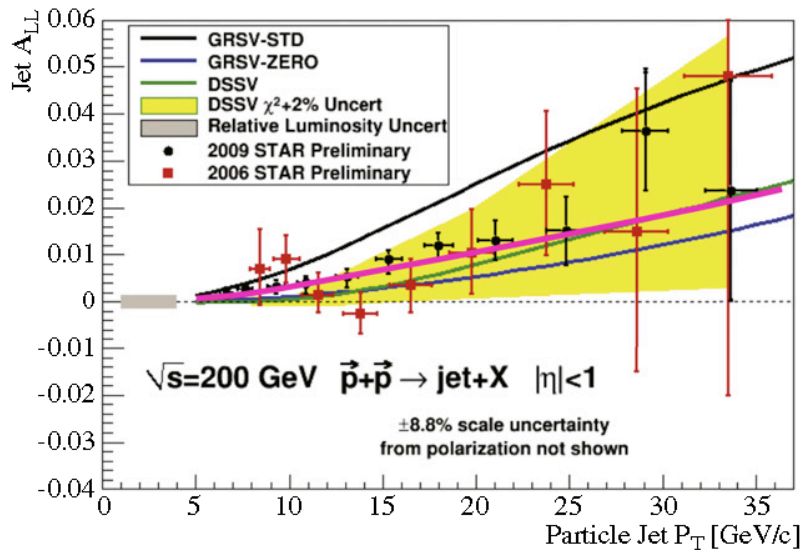


**Figure 3.11** STAR inclusive jet  $A_{LL}$  measurements in 200 GeV  $pp$  collisions from Run 6 (red points, see also [12]) and Run 9 (black points, [11]). The black and green curves are the GRSV-STD and DSSV 2008 [8] predictions. The yellow region is the  $\chi^2+2\%$  uncertainty region from the DSSV 2008 fit. The magenta curve shows a new preliminary fit [13] that includes the STAR preliminary Run 9 measurements.

Run 9 provided a major advance along this path. STAR once again measured  $A_{LL}$  for inclusive jet production in  $pp$  collisions at  $\sqrt{s} = 200$  GeV. The preliminary results [11] are a factor of 3 (at high  $p_T$ ) to >4 (at low  $p_T$ ) more precise than the Run 6 measurements [12]. The Run 9 inclusive jet inclusive jet  $A_{LL}$  measurements draw a narrow road through the DSSV uncertainty band, as shown in Fig. 3.11. The Run 9  $A_{LL}$  results systematically fall above the previous DSSV best-fit expectation. de Florian *et al.* have performed a new preliminary global analysis [13] including the preliminary Run 9 inclusive jet results from STAR, as well as preliminary Run 9 inclusive  $\pi^0$  results from PHENIX. The magenta curve in Fig. 3.11 is the outcome. It describes the STAR (and PHENIX) data quite well. The integral of  $\Delta g$  over the range  $0.05 < x < 0.2$  is 0.13 at

$Q^2 = 10 \text{ GeV}^2$ . de Florian *et al.* conclude, “Despite the fact that this really is only an illustration that cannot replace a proper re-analysis of the data, it does appear that, for the first time, there are indications of non-vanishing gluon polarization in the nucleon.” Within the past year, we have also performed our own fits within STAR, utilizing the DSSV code. Those fits indicate that the precision and kinematic reach of the STAR data are now sufficient so that they also provide the dominant constraints on the gluon polarization for  $x > 0.2$ .

STAR did not restrict itself to inclusive jets during Run 9. Figure 3.12 shows the preliminary STAR Run 9 results for  $A_{LL}$  for di-jets in 200 GeV  $pp$  collisions, separated into three different kinematic regions. The measurements fall somewhat above the predictions from the DSSV 2008 best-fit, consistent with the conclusions from the inclusive jets measurement. The statistics for di-jets are limited compared to inclusive jets. Nonetheless, di-jets provide a very valuable complement. For any given  $p_T$  bin, inclusive jet measurements average over a very broad  $x$  range. In contrast, di-jets permit a leading-order calculation of the incident parton kinematics on an event-by-event basis. This dramatically reduces the  $x$  range that is sampled within a single mass bin, as illustrated in Fig. 3.12. Thus, di-jets provide a direct experimental determination of the shape of  $\Delta g(x)$ , which is essential to minimize the uncertainties that arise when extrapolating the gluon polarization outside the  $x$  region that is sampled at RHIC.

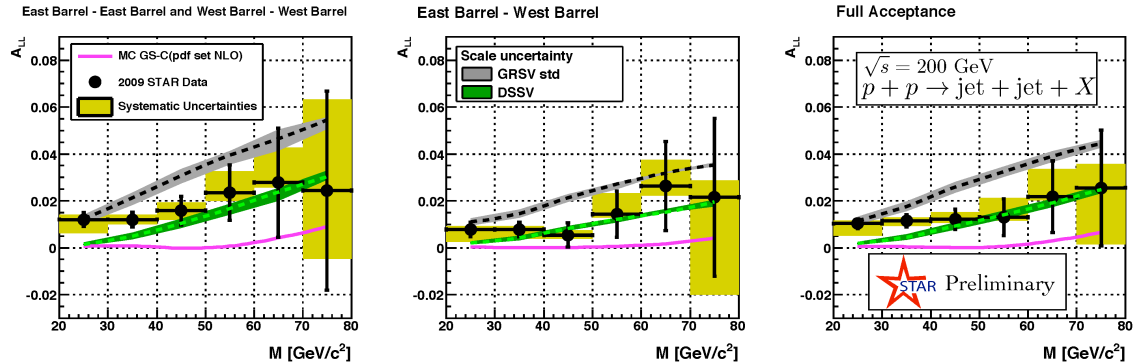


**Figure 3.12** STAR preliminary di-jet  $A_{LL}$  from Run 9 200 GeV  $pp$  collisions for three different kinematic regions [14].

We are continuing our Run 9 analysis in order to improve and extend these preliminary results. In the preliminary inclusive jet measurement, the systematic uncertainties associated with trigger and reconstruction bias are comparable to the statistical uncertainties in several jet  $p_T$  bins. We are exploring ways to minimize these systematic effects. We have found that the trigger and reconstruction bias uncertainty can be reduced substantially at the expense of a modest reduction in the overall jet statistics. At present, we are working to optimize the trade-off between statistics and systematics to obtain the smallest total uncertainties. The di-jet measurement in Fig. 3.12 required both jets to fall within  $|\eta| < 0.8$ . If we extend the pseudorapidity coverage to larger  $\eta$  for one or both jets, we will gain access to more asymmetric partonic collisions, thereby pushing the  $x$  coverage to lower  $x$  values than shown in the middle

panel of Fig. 3.13. The STAR Endcap EMC provides measurements of the neutral energy in jets out to  $\eta = 2$ . In contrast, the TPC tracking efficiency drops rapidly for  $\eta > \sim 1.3$ . The latter distorts the jet energy measurements and can bias the measurement of the jet thrust axis. Simulations indicate that the former has a larger impact on the reconstruction of the di-jet kinematics than the latter does. We are currently developing algorithms to combine information from the two jets in a way that minimizes fluctuations in the reconstructed di-jet properties.

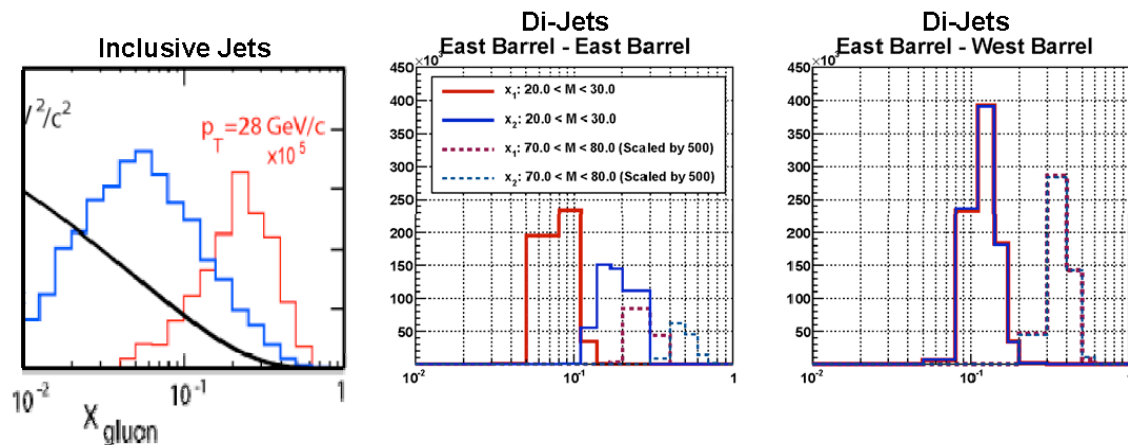


**Figure 3.13** The  $x$  ranges that are sampled by inclusive and di-jet measurements. The left panel shows the ranges for two inclusive jet  $p_T$  bins from Run 5 [15]. The middle and right panels show the ranges for two di-jet mass bins from Run 9 [14]. Note that, for the middle panel which involves asymmetric partonic collisions,  $x_2$  ( $x_1$ ) is the lower (higher) of the two momentum fractions.

The  $\sqrt{s} = 510$  GeV period of Run 12 was very successful, as discussed above in the Run 12 spin summary. The higher center-of-mass energy will allow us to extend our gluon polarization measurements to lower  $x$ , where the gluon density is quite large. As seen in Fig.3.6, we expect the data STAR recorded will determine  $A_{LL}$  for inclusive jets over the range  $0.03 < x_T (=2p_T/\sqrt{s}) < 0.1$  with statistical precision of  $\pm 0.002$  or better. We will also use the 510 GeV data from Run 12 to extend our measurement of  $A_{LL}$  for di-jet production to smaller  $x$ . The expected precision for di-jets can be inferred by scaling figure 3.14.

Figure 3.14 shows the precision that STAR will achieve during Run 13 for  $A_{LL}$  for di-jet production in polarized  $pp$  collisions with a data sample  $P^dL = 15 \text{ pb}^{-1}$  at  $\sqrt{s} = 510$  GeV. When the data from Runs 12 and 13 are combined, the uncertainties will be  $\sim 18\%$  smaller than shown in Fig. 3.14. Furthermore, only cases with at least one jet in the range  $|\eta| < 1$  are shown in Fig. 3.14. The complete FGT will be operational during Run 13, which will extend the pseudorapidity range where STAR can perform accurate tracking. Although detailed simulations have not yet been performed, we expect this will allow us to reconstruct at least some di-jet events where both jets fall within the region  $1 < \eta < 2$  spanned by the EEMC. This will push our gluon polarization sensitivity to even lower  $x$ . We also hope to combine Runs 12 and 13 data to reduce the uncertainties for inclusive jet  $A_{LL}$  at 510 GeV. However, improvements for inclusive jets beyond Run 12 will depend strongly on the ultimate size of the systematic

uncertainties associated with trigger and reconstruction bias and the relative luminosity determination.

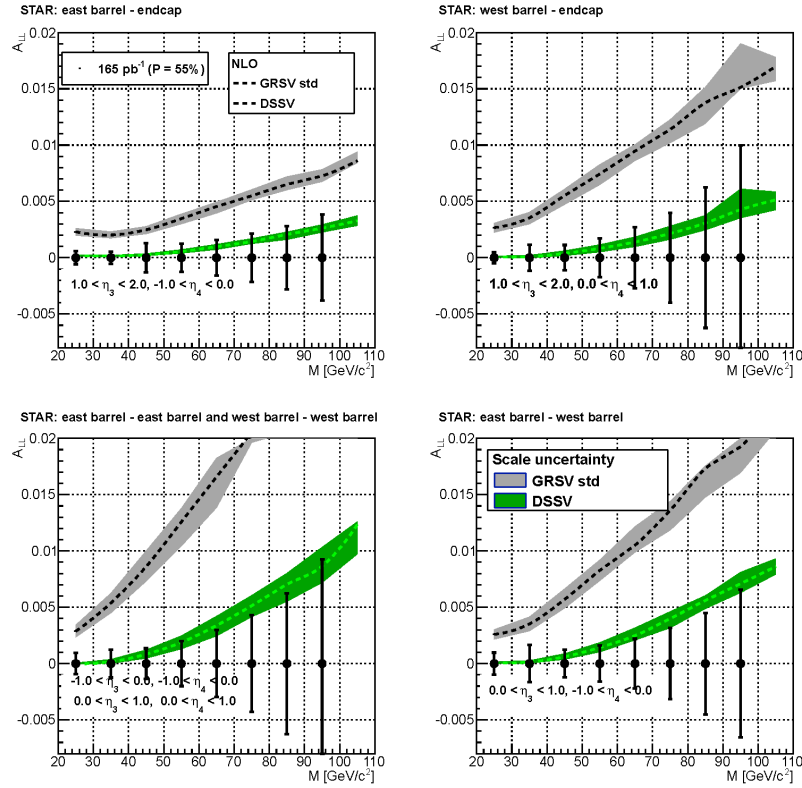


**Figure 3.14** Projected uncertainties for  $A_{LL}$  for di-jet production from Run 13. The green and gray curves show NLO calculations using DSSV 2008 and GRSV-STD, respectively. The widths of the bands indicate the scale uncertainties in the calculations. The uncertainties will be larger by  $\sim 40\%$  for Run 12, and smaller by  $\sim 18\%$  when the results from Runs 12 and 13 are combined.

The combination of inclusive and di-jet  $A_{LL}$  measurements in 200 and 510 GeV  $pp$  collisions will provide a far more detailed picture of the gluon polarization within the proton. Direct measurements will span the  $x$  range from below 0.02 to above 0.3, with very good precision over the lower half of that range and lesser precision in the upper half. Future 200 GeV data will extend the region with high-precision measurements to the upper half of the  $x$  range, as discussed in the Run 14 request below. Furthermore, the di-jet constraints on the shape of  $\Delta g(x)$  will enable reliable extrapolations outside the directly measured region. Together, these measurements will answer the question whether or not gluons “have appreciable polarization” in the range  $0.01 < x < 0.3$ .

### 3.5 Run 14 Request for 200 GeV Polarized p+p Collisions

STAR aims to significantly improve its gluon polarization measurements at  $\sqrt{s} = 200$  GeV concurrent with the accumulation of proton-proton reference data for the HFT and

MTD physics programs. The goal is to sample an additional  $40 \text{ pb}^{-1}$  with 65% longitudinal polarization in Run 14, making optimal use of the anticipated RHIC luminosity improvement afforded by the electron lenses.

Preliminary results, obtained in Run 9, on the double-spin asymmetry  $A_{LL}$  in inclusive jet production at  $\sqrt{s} = 200 \text{ GeV}$  from  $20 \text{ pb}^{-1}$  sampled with 58% average beam polarization are shown in figure 3.11. The data with transverse momenta larger than  $\sim 12 \text{ GeV}/c$  are statistics and hence luminosity limited. The DSSV extraction [7] is shown as well, together with the 3-4 times less precise data from Run 6. The latter data are one of the inputs to the DSSV fit and provide unique sensitivity to the polarized gluon distribution for  $0.02 < x < 0.2$ . Even though the Run 9 data have, to date, not been included in a full update of the DSSV analysis, their high qualitative impact is easily assessed and a preliminary evaluation [13] has revealed for the first time the existence of a positive contribution from gluon spin to the proton spin at the level of 0.1 in the kinematic range accessed at RHIC.

Further improvement in the uncertainties is thus of particular interest. A reduction by a factor of nearly 2 is achievable at high  $p_T > \sim 12 \text{ GeV}/c$  while a smaller improvement by about  $\sqrt{2}$  is still achievable at smaller  $p_T$ . Doing so would provide significant further constraints on the polarized gluon distribution, especially for large momentum fractions  $x$ , and constitutes the main spin physics objective for Run 14. The anticipated improvement and their complementarity with  $\sqrt{s} = 500 \text{ GeV}$  data are shown in figure 3.15.

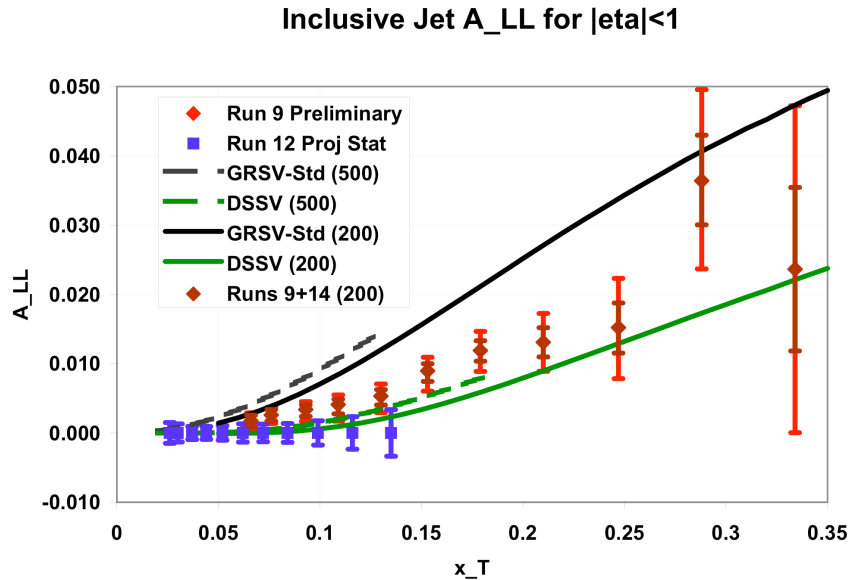


**Figure 3.15** The expected precision for  $A_{LL}$  vs.  $p_T$  for inclusive jets at  $\sqrt{s} = 200 \text{ GeV}$  p+p collisions after the proposed Run 14 data are combined with the existing Run 9 measurements (brown diamonds). Also shown are the current Run 9 results (red diamonds) and the expected precision at  $\sqrt{s} = 500 \text{ GeV}$  from Run 12 (blue squares), together with model predictions for both energies from GRSV-Std and DSSV 2008.

A new data set of  $40\text{pb}^{-1}$  with 65% longitudinal polarization will also lead to significant improvement over the preliminary STAR measurements of di-jet  $A_{LL}$  at  $\sqrt{s} = 200$  GeV. Important new results at with transverse beam polarization have recently been obtained at central-rapidity as well, as discussed in section 3.2. Analysis of the significantly larger  $\sqrt{s} = 200$  GeV data sample obtained in Run 12 will commence. Depending on progress and outcome, STAR may consider also continued running with transverse polarization in Run 14.

## References:

1. M. Aggarwal *et al.* (STAR Collaboration), Phys. Rev. Lett. **106**, 062002 (2011), arXiv: 1009.0326 [hep-ex].
2. A. Agakishiev *et al.* (STAR Collaboration), accepted for publication in Phys. Rev. D, arXiv:1112.2980 [hep-ex].
3. K. Melnikov and F. Petriello, Phys. Rev. D **74**, 114017 (2006), arXiv:hep-ph/0609070.
4. A. Martin, W. Stirling, R. Thorne, and G. Watt, Eur. Phys. J. **C63**, 189 (2009), arXiv: 0901.0002 [hep-ph].
5. B. I. Abelev *et al.* (STAR Collaboration), Phys. Rev. Lett. **101**, 222001 (2008), arXiv: 0801.2990 [hep-ex].
6. K. Kanazawa and Y. Koike, Phys. Rev. D **83**, 114024 (2011).
7. D. de Florian, R. Sassot, M. Stratmann, and W. Vogelsang, Phys. Rev. Lett. **101**, 072001 (2008) and Phys. Rev. D **80**, 034040 (2009).
8. E.A. Hawker *et al.*, Phys. Rev. Lett. **80**, 3715 (1998); R.S. Towell *et al.*, Phys. Rev. D **64**, 052002 (2001).
9. D. de Florian, R. Sassot, M. Stratmann, and W. Vogelsang, Phys. Rev. Lett. **101**, 072001 (2008); Phys. Rev. D **80**, 034030 (2009).
10. M.M. Aggarwal *et al.*, Phys. Rev. Lett. **106**, 062002 (2011).
11. P. Djawocho *et al.*, arXiv:1106.5769.
12. L. Adamczyk *et al.* arXiv:1205.2735.
13. D. de Florian, R. Sassot, M. Stratmann, and W. Vogelsang, Prog. Nucl. Part. Phys. **67**, 251 (2012).
14. M. Walker *et al.*, arXiv:1107.0917.
15. B.I. Abelev *et al.*, Phys. Rev. Lett. **100**, 232003 (2008).

## 4. Physics with Tagged Forward Protons at STAR

### 4.1 Executive Summary

We are requesting four days of beam time with transverse polarization at  $\sqrt{s} = 510$  GeV to investigate the non-perturbative regime of QCD at RHIC using the STAR detector and the Roman Pots of the pp2pp experiment [1-5]. The pp2pp Roman Pot detectors, already installed and used in Run 9, will be used again to tag very forward protons, thus selecting processes, in which the protons stay intact. The dominant amplitude of the exchange process has quantum numbers of the vacuum, so called Pomeron (IP) exchange. In Fig. 4.1 the Feynman diagrams of the investigated processes are shown together with corresponding diagrams in terms of azimuthal angle vs. pseudorapidity ( $\phi$  vs.  $\eta$ ).

The highest priority of our request is to fully characterize the proton-proton elastic cross section  $d\sigma/dt$  in the four-momentum transfer  $t$  range [0.02, 0.18] (GeV/c)<sup>2</sup>. Measuring pp elastic in this range will yield the first measurements at  $\sqrt{s} = 510$  GeV of the slope parameter of the elastic cross section  $B$ , and the total cross section,  $\sigma_{\text{tot}}$ . We will also acquire a sample of Central Exclusive Production (CEP) events, which would be by a factor of 30 to 40 bigger than in Run 9, thus allowing an analysis of a resonant structure in the two-pion invariant mass spectrum  $M_X$ , see Fig. 4.1b.

Using the capacity of existing power supplies special optics of  $\beta^* = 7.5$  m at  $\sqrt{s} = 510$  GeV can be produced allowing the coverage of small  $t$  for elastic scattering.

Based on our experience from run 9 we estimate our needs for about ten shifts of accelerator time (five shifts of beam time) as follows: 1) Beam development is about 2 shifts, confirmed by Wolfram Fischer; 2) Luminosity  $\sim 1.5 \times 10^{30} \text{cm}^{-2} \text{sec}^{-1}$  at  $\sqrt{s}=510$  GeV obtained by scaling measured luminosity in Run 9 of  $2 \times 10^{29} \text{cm}^{-2} \text{sec}^{-1}$  to the proposed conditions in Run 13; 3) Data taking 3 shifts at  $\sqrt{s} = 510$  GeV for elastic and CEP totaling five shifts of data taking, with 50% overall efficiency of data taking will result in 10 shifts or about four days of accelerator time; 4) CEP rate about 100-200 Hz, would allow for 20-30 times larger statistics than that collected during run 2009, allowing more quantitative analysis of the  $M_X$  plot obtained in Run 9; 5); As during Run 9 beam scraping to reach smallest  $t$  possible and Vernier scans to measure luminosity will be needed; 6) If possible, we shall ask for one shift of APEX to measure optics using Roman Pots (has been done at the LHC) and for which there is an interest in C - AD.

Our measurement of the total cross section,  $\sigma_{\text{tot}}$ , at the top of RHIC  $\sqrt{s}$  range, at which only a small difference of  $\sigma_{\text{tot}}$  between pp and p  $\bar{p}$  is expected, will probe the prevalent assumption that their scattering is asymptotically identical.

The instantaneous luminosity at PHENIX as shown in Table 4.1, will be about  $2 \times 10^{31} \text{cm}^2 \text{sec}^{-1}$ , which is obtained by scaling luminosity at STAR by the ratio of the  $\beta^*=7.5\text{m}$  function at STAR and PHENIX:  $7.5\text{m}/0.6\text{m}=12.5$ .

We propose to have the pp2pp four-day run at the beginning of the Run 13 510 GeV pp running period. The luminosity tends to be lower at the beginning, which has much less impact on the pp2pp program than on the W and  $\Delta g$  measurements. This will also give C-AD more time behind RHIC stores early in the run to gain experience with the new polarized source, which might increase the Figure of Merit delivered later.

## 4.2 Physics Motivation

There are two main reactions that can be studied with tagged forward protons: polarized proton-proton elastic scattering and Central Exclusive Production (CEP) in double Pomeron exchange (DPE); see Fig. 4.1.

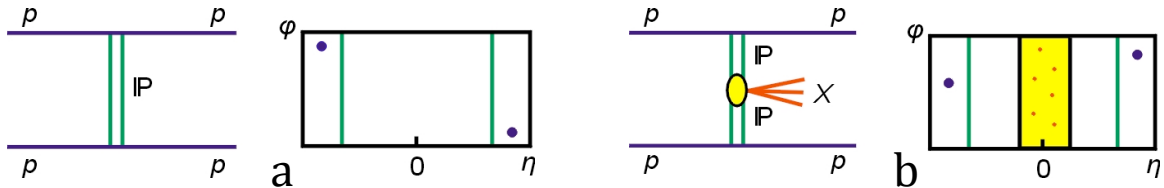


**Figure 4.1** a) Elastic Scattering diagram ; and b) Central Exclusive Production diagram. Feynman diagrams and corresponding azimuthal angle vs. pseudorapidity diagrams are also shown.

The measurements we propose using polarized proton beams at RHIC, the STAR detector and the Roman Pots of the pp2pp experiment [1-5] will help to investigate the non-perturbative regime of QCD. The pp2pp Roman Pot detectors, already installed and debugged during Run 9, will be used to tag very forward protons, thus selecting processes, in which the proton stays intact, see Fig.4.1. The mechanism of particle production in the central rapidity region is dominated by double Pomeron exchange and thus believed to enhance glueball formation. The use of polarized proton beams, unique at RHIC, will allow exploring unknown spin dependence of diffraction including both elastic and inelastic processes [6-8].

**Elastic Scattering:** The entire energy range of this proposal has been inaccessible in proton-proton (elastic) scattering up to date, hence new results of high quality that can be obtained at RHIC on  $\sigma_{\text{tot}}$  and B are very important to understand the behavior of those fundamental quantities as a function of  $\sqrt{s}$ . The summary of existing data on pp and p  $\bar{p}$  total, elastic and inelastic cross sections is shown in Fig. 4.2, which includes recently published result from the TOTEM experiment at the LHC [10].

Of particular interest is difference between the total cross sections for pp and p  $\bar{p}$ , which could be explained by a contribution of the Odderon to the scattering amplitude. The absence of an Odderon contribution would lead to identical cross sections, which is why the measurement at the highest RHIC cms energy  $\sqrt{s}=510$  GeV is important. The

measurement of the differential pp elastic cross section  $d\sigma/dt$  over the extended  $t$ -range will allow measurement of the nuclear slope parameter  $B$  in a fit to the differential cross section and the total cross section  $\sigma_{\text{tot}}$ .

Since the difference in  $\sigma_{\text{tot}}$  between for pp and p  $\bar{p}$  scattering is expected to be small at the top RHIC  $\sqrt{s}$  range, the measurement of the  $\sigma_{\text{tot}}$  at RHIC, where comparison with p  $\bar{p}$  is possible, will probe the prevalent assumption that the cross sections for pp and p  $\bar{p}$  scattering are asymptotically identical. With expected  $20 \cdot 10^6$  elastic events an estimated error on the slope parameter is  $\Delta B = 0.3 \text{ (GeV/c)}^{-2}$  and  $\Delta \sigma_{\text{tot}} \approx 2 \text{ mb}$ .

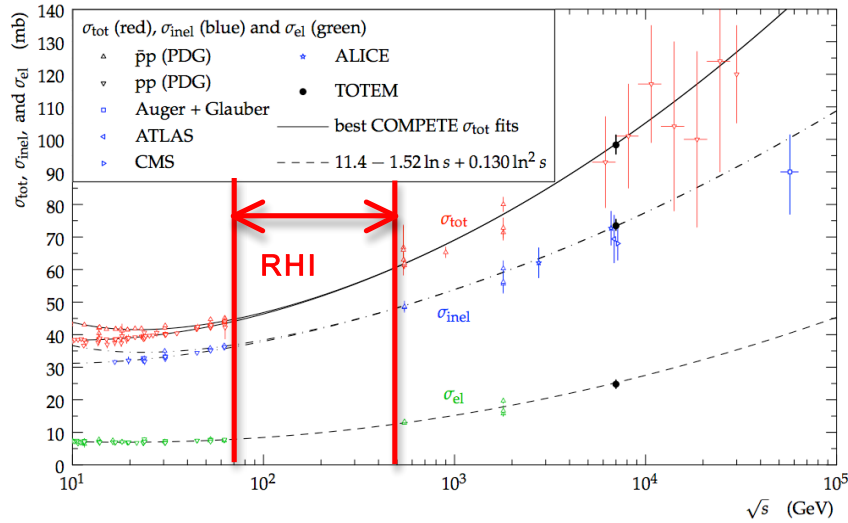


**Figure 4.2** The summary of existing data on pp and p  $\bar{p}$  total, elastic and inelastic cross sections [10].

**Spin dependent observables:** The availability of transverse polarization at STAR would allow measuring  $A_{NN}$ ,  $A_{SS}$ , and  $A_N$  resulting in a significant improvement of our physics capabilities. These measurements will complement results obtained in Run 9 for the  $t$ -values in the Coulomb Nuclear Interference (CNI) region where the spin-flip effects due to the hadronic interaction were found to be compatible with zero [9].

**Central Exclusive Production (CEP) in proton – proton collisions:** Tagging and measuring the forward protons is important since it removes the ambiguity of a (complementary) rapidity gap tag, which has a background due to the low multiplicity of diffractive events, and allows the full characterization of the event in terms of  $t$ ,  $\xi$  and  $M_X$ . The momentum balance between the scattered protons and the centrally produced system, exclusivity condition, allows obtaining a relatively background free data sample, like the one obtained in Run 9 at  $\sqrt{s} = 200 \text{ GeV}$ , for which the statistics of the data sample was limited because of the luminosity and the  $t$ -range for that run.

In Fig.4.3 we show a preliminary measurement of the invariant mass spectrum of the  $\pi^+\pi^-$  pairs produced in the exclusive process  $pp \rightarrow pXp$  (CEP), obtained with the STAR detector at RHIC at  $\sqrt{s} = 200 \text{ GeV}$ . The Roman Pots were used to tag forward protons

and the invariant mass of the pion pair was obtained using tracks reconstructed in the STAR Time Projection Chamber (TPC). To select CEP events the balance of momenta of the outgoing protons and central  $\pi^+\pi^-$  pair was required. These events can be seen in Fig. 4.3a) as a diagonal band. The resulting distribution of invariant mass of the central pair for the selected CEP events is displayed in Fig. 4.3b), which also shows a very small non-exclusive background estimated from events with like-sign charge pairs.

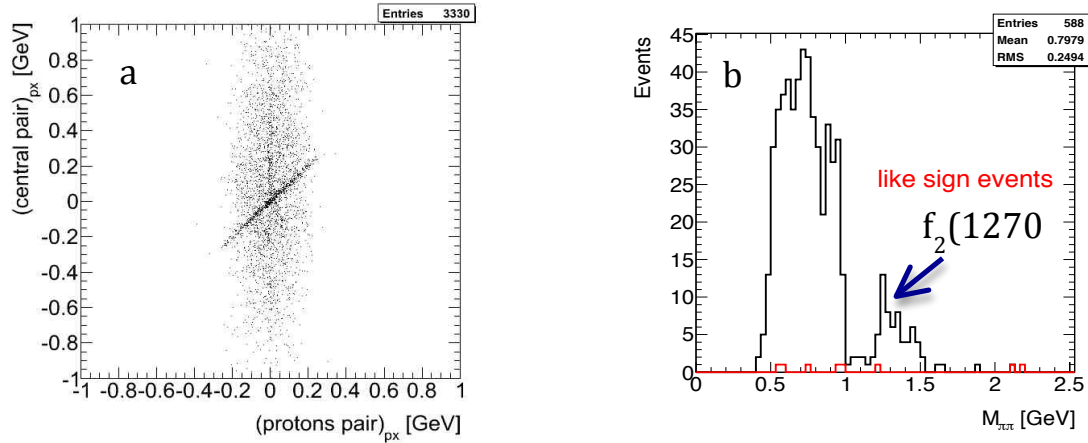


**Figure 4.3** a) Transverse momentum correlation of the  $\pi^+\pi^-$  pairs measured in the STAR TPC vs transverse proton pair momentum measured in the Roman Pots; b) Invariant mass of the  $\pi^+\pi^-$  pairs using the events in the correlation band, a small background of like sign  $\pi\pi$  pairs events, in red, is also shown.

During Run 13 we expect to collect a data sample in a wider  $t$  range, allowing for 30 – 40 times larger statistics as compared to that in Fig. 4.3b). Thus allowing a detailed study of the structure seen there.

**Triggers:** Triggers in Run 13 will be the same as in Run 9. We shall use elastic and inelastic trigger bits (ET, IT) based on scintillation counters mounted in the Roman Pots. The CEP trigger is an “and” of Time of Flight (ToF) multiplicity and inelastic trigger in the Roman Pots.

### 4.3 Run 13 pp2pp Request

We are requesting a four-day run with special running conditions during Run 13 with transverse polarization. Thus allowing us to acquire sizeable data samples for our program of elastic scattering and CEP. The main reason for special conditions is that in order to reach the  $t$  and  $\xi$  values needed for both diffractive and elastic data, the beam scraping and special optics of  $\beta^* = 7.5$  m are needed. The luminosity measurements, as in Run 9 will also be needed.

There are two major topics of interest, which will be studied: elastic scattering and central exclusive particle production in DPE processes. The expected performance is

shown in Table 4.1. The luminosity values were obtained scaling the performance of Run 9 measured performance.

The four-day run includes two shifts of beam commissioning and three shifts of data taking. We included efficiency factor of 50%, which takes into account that stores last longer due to the beam scraping. With the above conditions at least  $20 \times 10^6$  elastic events for analysis of elastic scattering, the single  $A_N$  and double  $A_{NN}$ ,  $A_{SS}$  spin asymmetries. An estimated error on the slope parameter is  $\Delta B = 0.31 \text{ (GeV/c)}^{-2}$ , the error on  $\sigma_{\text{tot}}$ ,  $\Delta \sigma_{\text{tot}} \approx 2 \text{ mb}$ .

Luminosity	$\text{cm}^{-2} \text{ sec}^{-1}$
STAR ( $\beta^*=7.5\text{m}$ )	$1.5 \times 10^{30}$
PHENIX ( $\beta^*=0.7\text{m}$ )	$2 \times 10^{31}$

**Table 4.1** Luminosities for pp2pp runs

We propose to take the pp2pp data at the beginning of the Run 13 510 GeV pp running period. The luminosity tends to be lower at the beginning, which has much less impact on the pp2pp program than on the W and  $\Delta g$  measurements. This will also give C-AD more time behind RHIC stores early in the run to gain experience with the new polarized source, which might increase the Figure of Merit delivered later.

## References

- 1) S. Bültmann et al., Phys. Lett. **B579** (2004) 245.
- 2) S. Bültmann et al., Nucl. Instr. Meth. **A535** (2004) 415.
- 3) S. Bültmann et al., Phys. Lett. **B632** (2006) 167.
- 4) S. Bültmann et al., Phys. Lett. **B647** (2007) 98.
- 5) W. Guryn et al., RHIC Proposal R7 (1994) (unpublished).
- 6) V. Barone, E. Predazzi, *High-Energy Particle Diffraction*, Texts and Monographs in Physics, Springer-Verlag (2002) ISBN: 3540421076.
- 7) S. Donnachie, G. Dosch, P. Landshoff, *Pomeron Physics and QCD*, Cambridge University Press (1998) ISBN: B0006Z3XLM.
- 8) A. Bravar, W. Guryn, S.R. Klein, D. Milstead, B. Surrow, J.Phys. **G28** (2002) 2885.
- 9) L. Adamczyk et al., the STAR collaboration “Single Spin Asymmetry  $A_N$  in Polarized Proton-Proton Elastic Collisions at  $\sqrt{s} = 200 \text{ GeV}$ ”, under review in the STAR collaboration.
- 10) G. Antchev et al., The TOTEM Collaboration, EPL, **96** (2011)21002.

## 5. Study of the Properties of QGP at RHIC Top Energy

### 5.1 Run 13 Heavy Ion Request

For Run 13, there will be a partial installation of the Muon Telescope Detector (MTD) and Heavy Flavor Tracker (HFT). The MTD has as a milestone installation to 43% coverage, though it is likely that a larger fraction will be complete. The electronics readout and triggering chain have been fully tested and vetted in Run 12 and before, so the additional modules will be rapidly commissioned for use at full physics quality in Run 13. For the HFT, this will be the first run in which the readout technology is integrated into STAR, and the installed coverage will be a few high precision PXL ladders without the intermediate layers of the IST and SSD to connect tracks from the TPC to the PXL. Because of this, for the HFT STAR views Run 13 as an engineering run to prepare for successful use of the full system in Run 14.

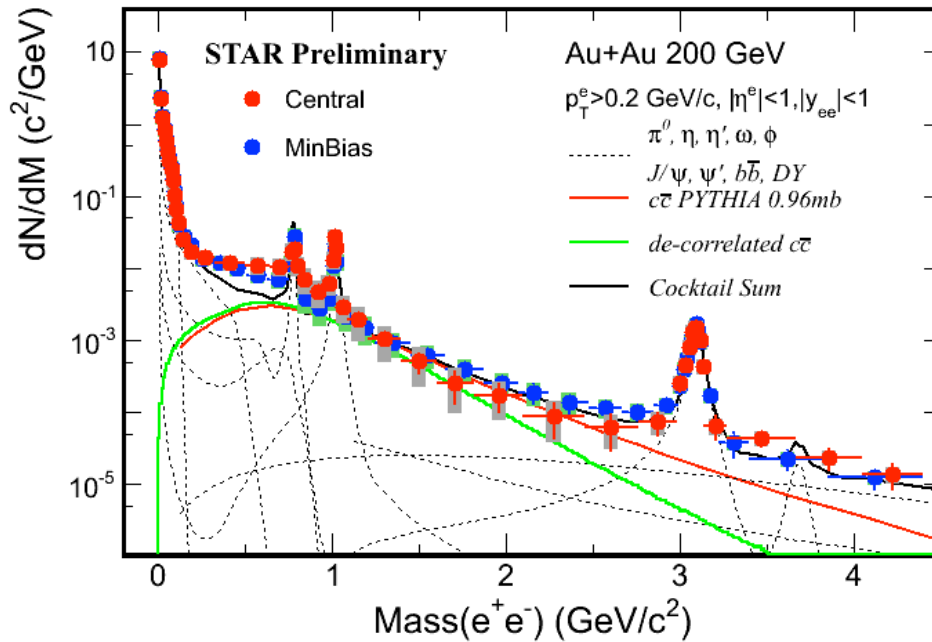


**Figure 5.1** Central and minimum bias di-electron invariant mass distributions, from Run 10 Au+Au. Central data has been scaled to match minimum bias at low invariant mass. Red line shows the cocktail contribution from fully correlated charm-anticharm pairs, assuming a cross section of 0.96 mb. Green line shows the contribution if charm is angularly decorrelated and momentum distributions softened to match non-photonic electron  $R_{AA}$ .

Despite the partial coverage of the MTD, a Au+Au run in Run 13 at  $\sqrt{s_{NN}} = 200$  GeV can provide significant new measurements without parallel in previous runs or in other experiments at RHIC. Most notably, the MTD allows for the measurements of electron-muon correlations, where the electron and muon are both measured at mid-rapidity. The dominant source of these correlations at intermediate mass is from the decay of charm-anticharm pairs, since in thermal production of dilepton pairs electrons are paired with positrons, and muons with antimuons. In Run 12 p+p collisions at  $\sqrt{s}$

=200 GeV STAR established that we can trigger on electron-muon pairs with one leg in the MTD and the other leg in the Barrel Electromagnetic Calorimeter (BEMC) at a transverse energy threshold of 1.9 GeV. This was a very clean trigger, running at prescale 1 with a very low rate ( $\sim 10^3$  s of Hz), which sampled an integrated luminosity of  $23 \text{ pb}^{-1}$ . We expect that this trigger will be equally effective in Au+Au collisions, allowing us to sample the entire set of luminosity delivered by RHIC while STAR is taking data and the DAQ system is live. We can also sample a large fraction of the delivered luminosity with a central trigger, which enables the kinematic cuts to be relaxed to allow for lower energy electrons, identified via the ToF and TPC  $dE/dx$ .

Figure 5.1 shows the existing minimum bias and central di-electron pair invariant mass distributions, where the central data has been scaled to match the minimum bias data at low invariant mass. According to the cocktail, the correlated charm contribution dominates the contribution in the intermediate mass range from 1 to 3  $\text{GeV}/c^2$ . In this figure, the correlated charm contribution is from PYTHIA, assuming no decorrelation in medium and rescaled to match a charm cross section of 0.96 mb. Both of these assumptions introduce a large uncertainty, due to the possibility of charm energy loss and decorrelation in the medium, both of which would decrease the contribution in this mass range. There are hints of suppression in central as compared to minimum-bias data, but at the level of this measurement these remain only hints. This uncertainty prevents the extraction of any signal from QGP radiation, which in the absence of decorrelation is approximately an order of magnitude below the charm contribution. The only way to make progress is to directly measure the correlated charm contribution in heavy ion collisions: electron-muon correlations provide one method to do so.

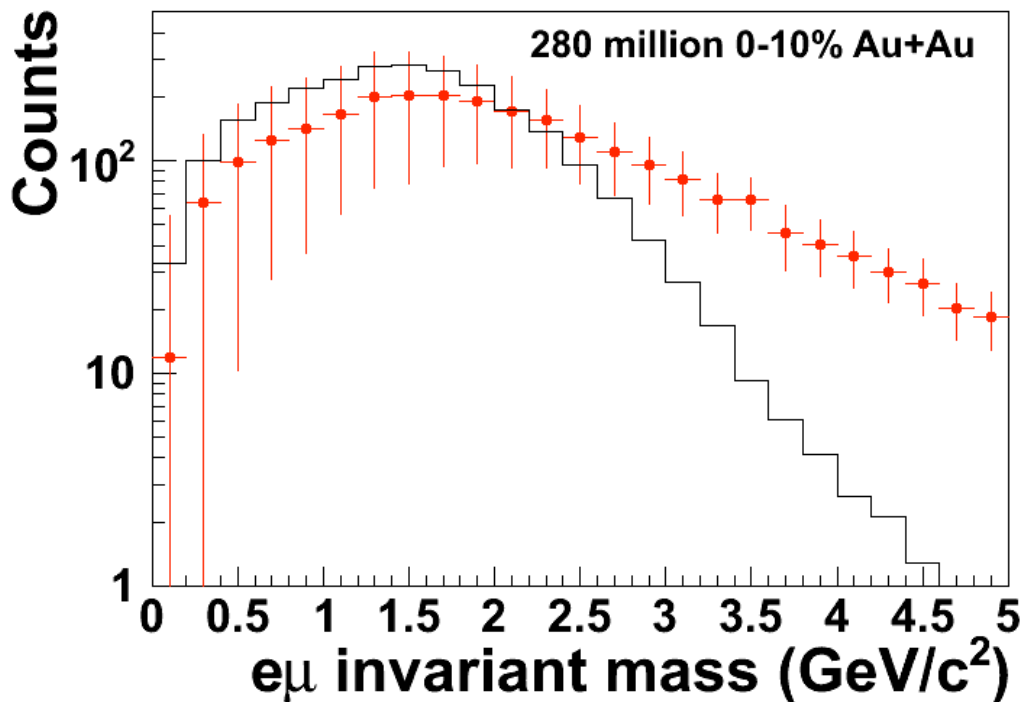


**Figure 5.2** Projected electron-muon invariant mass distribution from 280M 0-10% central Au+Au events and MTD coverage as in Run 13. Red points assume full

correlation and momentum distributions from PYTHIA, while the black curve assumes full decorrelation and softening of the charm momentum distribution to match non-photonic electron  $R_{AA}$ .

Figure 5.2 shows the projected uncertainty in the electron-muon invariant mass distribution for 280M central 0-10% Au+Au events, assuming the PYTHIA fully correlated charm contribution. For comparison, the black histogram shows the maximal reduction in the distribution, assuming full angular decorrelation and suppression of the charm singles distribution following measured non-photonic electron  $R_{AA}$ . The proposed measurement can clearly distinguish this extreme scenario from the fully correlated PYTHIA scenario. 280M events need approximately 200 DAQ hours at 400 Hz, or three weeks of running at historical running efficiencies of RHIC and STAR. If the correlated charm signal is maximally reduced, with this dataset a first measurement of QGP radiation at intermediate mass will be possible, with limited precision. Longer runs will be necessary to extract the QGP radiation signal with precision.

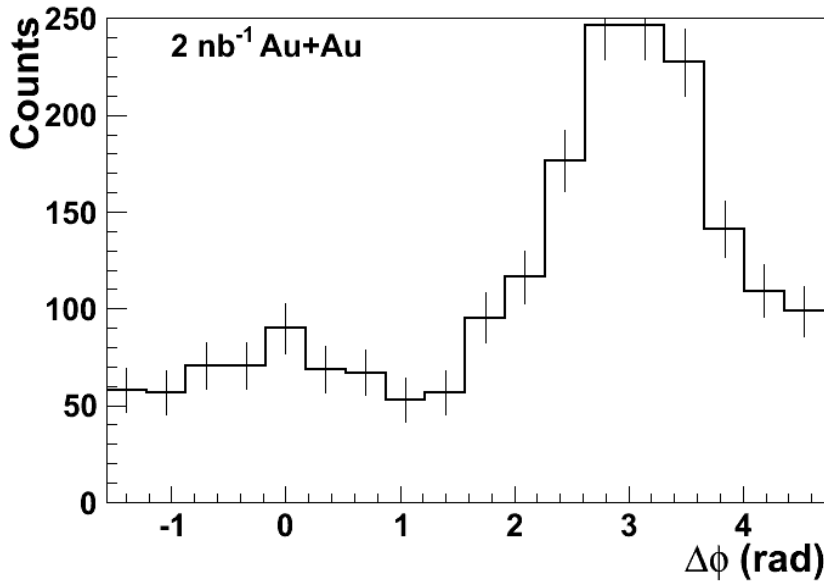


**Figure 5.3** Projected electron-muon  $\Delta\phi$  distribution for electron  $p_T > 2$  GeV/c, for  $2 \text{ nb}^{-1}$  Au+Au sampled by a trigger between an MTD hit on one leg and an electron in the Barrel Electromagnetic Calorimeter with  $E_T > 1.9$  GeV/c.

The downside of such triggered datasets is that they select specific regions of the invariant mass vs.  $p_T$  plane, and so need detailed comparisons with unbiased data and simulations under energy loss scenarios to interpret correctly. As a starting point, Figure 5.3 shows the projected uncertainty on the  $\Delta\phi$  distribution between the electron and muon, with electron and muon  $p_T > 2$  GeV/c, with the expected strength of the correlation from PYTHIA, after sampling  $2 \text{ nb}^{-1}$  with the MTD-BEMC trigger as run in Run 12. This sample could be obtained in three weeks, in parallel with the central sample. Angular decorrelation of charm-anticharm pairs would lead to a decrease of

the height and/or broadening of the width of the away-side peak, which is clearly resolvable with this sample.

For the Heavy Flavor Tracker, some time with Au+Au beams would be extremely useful for commissioning and producing real-world verification of the performance of the detector. With only partial angular coverage of the PXL and without the intermediate tracking layers of the SSD and IST to cross the large difference in resolution between the TPC and the PXL, the PXL layers will have to rely on the vertex position much more in the engineering run configuration than in the final HFT configuration. The vertex position is much better constrained in a central Au+Au event than in a p+p event, because of the  $1/\sqrt{N_{\text{track}}}$  improvement in the vertex resolution. One goal of the commissioning is to fully vet the software chain to verify the ability to reconstruct displaced vertices to the required resolution; realistically, this goal can only be fully accomplished with Au+Au beams.

Beyond that, much can be done with the HFT with other beam combinations. An engineering run with the HFT PXL detector serves a number of important functions that are required in the development of a robust detector system capable of producing useful physics in a timely fashion. Some functions address resolution of questions that could affect or require modification of the final design. Other functions address the need to get an early start on hardware and software commissioning in order to guarantee physics results from the first run with the HFT. This is particularly important in the current scenarios that has proposed short run-13 and run-14.

The engineering run will provide a test for vulnerability to wakefield generated noise or other unanticipated noise sources. We don't expect this to be an issue with our detector design, but if the engineering run exposes a problem then RF shielding would be implemented.

The PXL detector electronics system, detector plus read out, will be tested with the STAR DAQ and trigger system prior to the engineering run so integration complications are not expected, but the engineering run could reveal unexpected issues with pickup or grounding associated with DAQ connections that would require correction prior to the complete HFT operation.

The proposed engineering run will test software for detector alignment through tracking so that good working software is available at the start of operation of the complete HFT detector system. The engineering run will be an important time for commissioning this software as well as other software systems such as slow controls and various diagnostic software tools. There are many such functions that will require testing and correction that can be accomplished only through actual operation. Experience has repeatedly and painfully shown that bringing up a new detector system in a collider environment is a daunting task with many time conflicting activities which are still all essential to proper operation. It is important to recognize this and design an engineering run to provide an ordered approach to commissioning the detector.

Also the full trial assembly sequence of the Inner Detector Support with Main Support Cone, but without the added hassle of also requiring full integration and assembly of SSD and IST is of great value. There is a lot of structures to come together, and having a trial dry fit of all, together, with the new small beam pipe, a full year before they are fully required to meet physics run requirements, allows us ample time to fix, adjust, or otherwise modify structures required to support IST, Pixels and the new beam pipe. Pixel insertion in the STAR Hall is no small task. Having the MSC installed, with new beam pipe, in STAR WAH, will allow verification of all external installation tooling, and potential interferences, again allows sufficient time for modification before installation ahead of run-14 (Summer/Fall) in 2013.

Though heavy ion collision is the preferred species for the engineering run many aspects can be addressed in a pp running mode. This would likely involve a number of shorter runs with reduced luminosity (by detuning the beam at STAR) in order to reduce the pile-up of tracks in the TPC and triggering on high multiplicity events to allow for multiple tracks within the reduced solid angle coverage.

Among the goals for data taking are

- Quantify Effects from beam condition on noise and hits in PXL instantaneous and over the course of the run.
- Identify issue with trigger and DAQ.
- Investigate the track matching between TPC and PXL layer 1 and 2.
- Investigate vertex pointing quality
- Commissioning of calibration and analysis software

For the engineering run only the PXL sub-system will be available. The PXL sectors can be installed into STAR during any longer access day using the insertion mechanism from the East end of STAR. Only a subset of the 10 sectors will be instrumented. Each sector consists of 4 ladders, one at  $\sim 2.5$  cm and 3 at 8 cm. Each ladders consists of 10  $2 \times 2$  cm CMOS sensors. The aim is to have 3 sectors instrumented, but the actual number will depend on the yield of fabrication of ladders. The aim is to have these ready by end of January 2013.

## 5.2 Run 14 Heavy Ion Request

In Run 14, the complete HFT and MTD will be installed and ready for physics. The primary goal from this run is to make first measurements in Au+Au collisions of directly reconstructed charm, to see whether charm flows at the low  $p_T$  where hydrodynamics is applicable. Figure 5.4 shows the projected errors on  $D^0 v_2$  in a sample of 500M minimum bias events, which can be collected in approximately 300 DAQ hours at a recording rate of 500 Hz.

With this dataset, the binary-scaled ratio of central to peripheral spectra,  $R_{CP}$ , for directly reconstructed  $D^0$  mesons can be measured out to 10 GeV, well into the region where the mass of the charm quark is small compared to  $p_T$ , and so tagging on charm is equivalent to tagging on the quark, and also to a  $p_T$  sufficient for a first attempt to

subtract the electrons from charm from the overall non-photonic electron spectrum. Measuring  $R_{AA}$ , rather than  $R_{CP}$ , requires a large untriggered dataset in p+p collisions at 200 GeV.

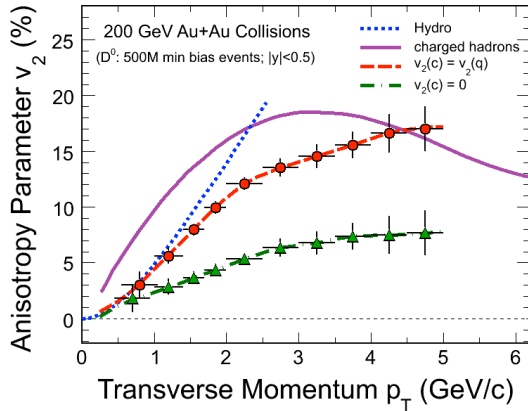


**Figure 5.4** Projection of  $D^0$   $v_2$ , as compared to hydrodynamical calculations and coalescence calculations assuming charm flows as light quarks, or does not flow.

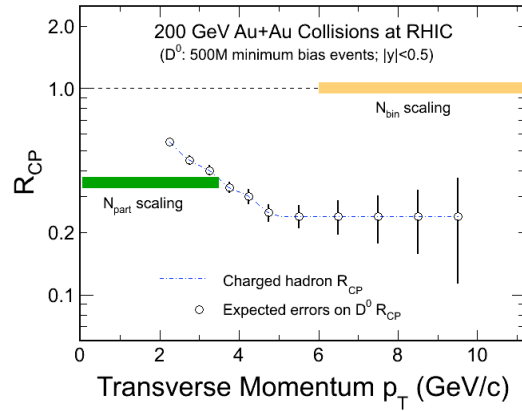


**Figure 5.5** Projected uncertainties on  $D^0$   $R_{CP}$

Using triggered datasets, first open beauty measurements in Au+Au collisions in STAR can be made using displaced electrons as shown in Figure 5.6. The ratio of electrons from beauty to those from charm, measured in Au+Au, can be compared to published STAR results from electron-hadron and electron- $D^0$  correlations in p+p collisions, to see if beauty is suppressed less than charm in medium at RHIC energies. The projection folds in the loss of luminosity due to the requirement of a tight vertex z cut in order to maximize the acceptance of the HFT PXL layers.

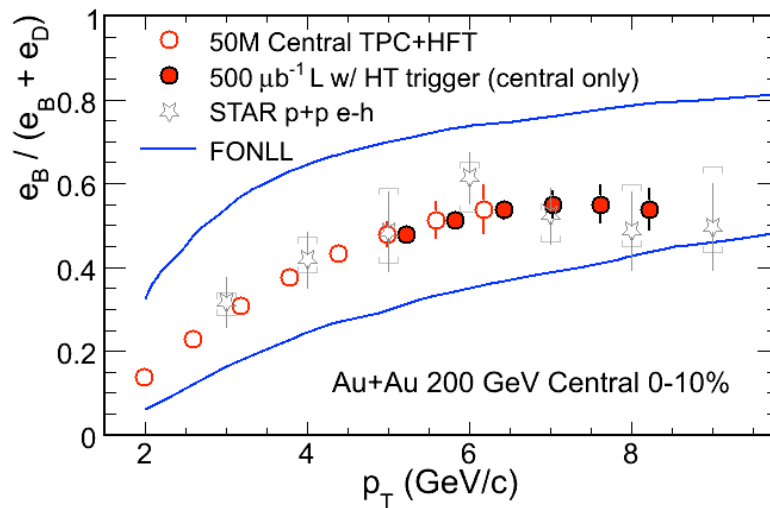


**Figure 5.6** Projected ratio of electrons from beauty to total non-photonic electrons in Au+Au collisions, for integrated luminosities and event counts as shown. For comparison, published results from p+p collisions are shown [STAR, Phys. Rev. Lett.

105 (2010) 202301], along with the band of allowed results from Fixed Order Next-to-Leading Log calculations in p+p collisions.

Run 14 will not allow for datasets of the size needed for tests of coalescence using the  $\Lambda_c$ . Figure 5.7 shows a projection of the uncertainties on the  $\Lambda_c$ , with a Minimum Bias dataset four times larger than that proposed for Run 14 plus a distinct central dataset five times larger than that enclosed in the Run 14 minimum bias dataset. This size of a dataset is needed to make definitive statements about whether charmed baryons are enhanced relative to charmed mesons, in direct analogy to the light hadron baryon/meson enhancements believed to be caused by the dominance of coalescence as a particle production mechanism. Since much of the interpretation of charm  $v_2$  at intermediate  $p_T$  hinges on the coalescence mechanism between flowing charm quarks and flowing light quarks enabling the two flows to add, this test of the coalescence mechanism is critical, and so STAR will need to return to Au+Au with the HFT after Run 14.

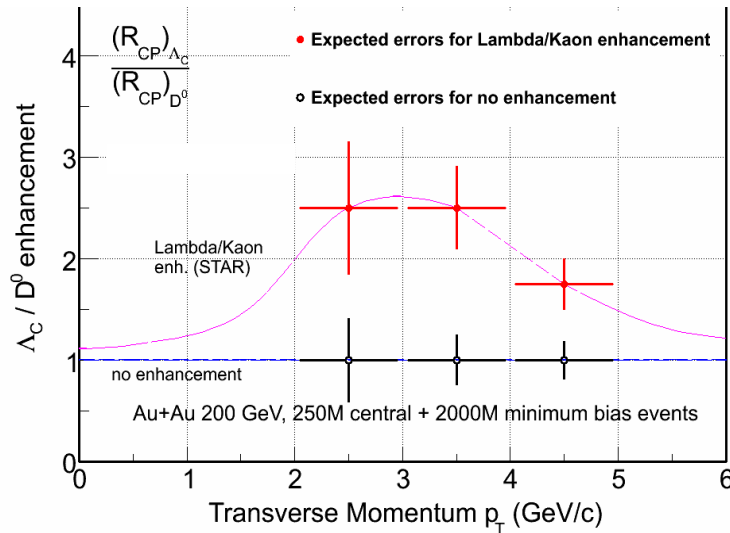


**Figure 5.7** Projected uncertainties on double ratio of  $(R_{CP} \Lambda_c)/(R_{CP} D^0)$  from a long Au+Au run, with datasets larger than can be obtained in Run 14.

Run 14 also begins the physics program with the full MTD. The primary focus of this program is on Quarkonia at RHIC energies, using muons to completely remove the issue of Bremsstrahlung tails in the lineshapes. This is most important in the separation of the Upsilon 1S from the 2S and 3S states, all three of which are expected to be suppressed differently in the QGP. Figure 5.8 shows a projected line-shape with the MTD, showing that the 1S can be clearly separated from the 2S+3S, while the 2S and 3S can be separated statistically assuming a large statistics sample and good control over the lineshape. Figure 5.9 shows the projected  $R_{AA}$  for the sum of the three states, as a measure of total statistical power. These measurements require a large integrated luminosity: to measure the  $R_{AA}$  of Upsilon 3S will be a multi-year program, and likely requires p+p running at  $\sqrt{s} = 500$  GeV, along with the assumption that the relative ratios of the Upsilon states do not change with  $\sqrt{s}$ , an assumption that world data supports. Table 5.1 shows an estimate for the required luminosity for measurements of the 2S+3S

and the 3S separately. Run 14 will likely allow for a separation of the 2S+3S from the 1S. But it will need to be followed by a long p+p reference run in order to obtain  $R_{AA}$ , and will need further Au+Au running for study of the 3S state itself.

Collision System	Minimum Luminosity for 10% uncertainty on Upsilon 3S	Minimum Luminosity for 10% uncertainty on Upsilon 2S+3S
p+p 200 GeV	420 pb <sup>-1</sup>	150 pb <sup>-1</sup>
p+p 500 GeV	140 pb <sup>-1</sup>	50 pb <sup>-1</sup>
Au+Au 200 GeV	10 nb <sup>-1</sup>	3.8 nb <sup>-1</sup>

**Table 5.1** Upsilon luminosity requirement estimation

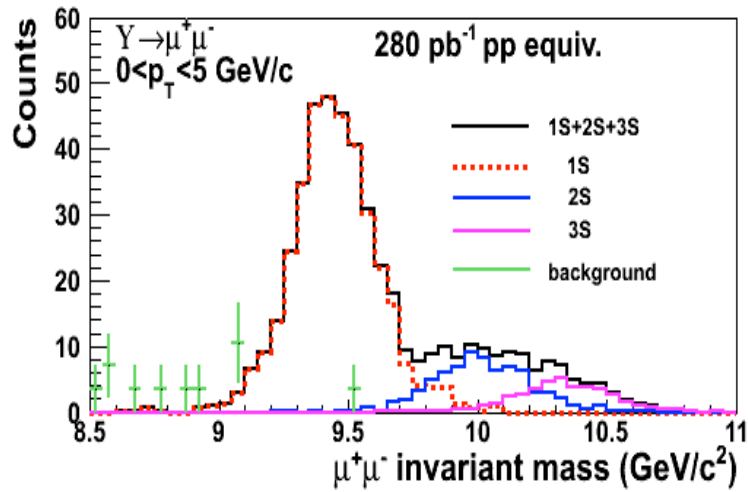


**Figure 5.8** Projected Upsilon line-shape in the MTD for the three separate states.

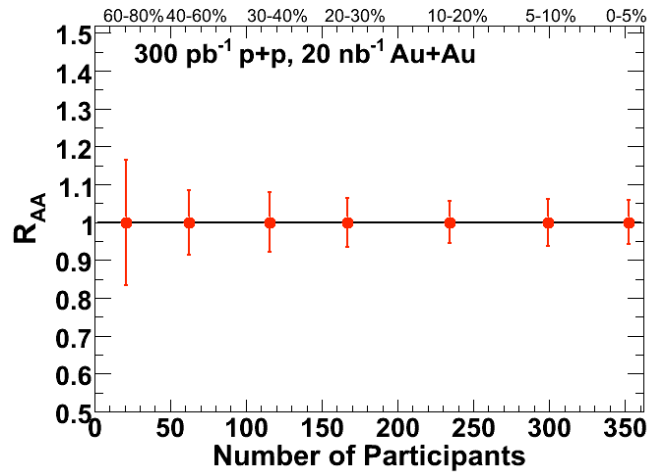


**Figure 5.9** Projected errors on  $R_{AA}$  of Upsilon 1S+2S+3S in the STAR MTD, after a multi-year program to accumulate sufficient luminosity.

### 5.3 Run 14 pp Reference Data Request

The STAR heavy flavor program also needs a p+p reference dataset at  $\sqrt{s}=200$  GeV, in order to make measurements of  $D^0$   $R_{AA}$  rather than  $R_{CP}$ . Theoretical calculations and past STAR measurements without the HFT are not of sufficient precision to produce a baseline, and it is theoretically cleaner to interpret  $R_{AA}$  than  $R_{CP}$ . Figure 5.10 shows the projected relative uncertainties on the measured  $D^0$   $p_T$  spectra with 500M p+p minimum bias and 50M 0-10% Au+Au central events that can be obtained in Run14. Note that 500M p+p events only consist part of the required reference dataset for the  $R_{AA}$  measurement. In order to have a comparable precision as in central Au+Au collisions at high  $p_T$ , we estimate a need for 2000M p+p minimum bias events, or approximately 1200 DAQ hours at 500 Hz, which will require a multiple years of  $\sqrt{s} = 200$  GeV p+p runs. For Upsilon  $R_{AA}$  measurement, in Run 14, we will collect  $40\text{pb}^{-1}\sqrt{s} = 200$  GeV collisions with MTD trigger.

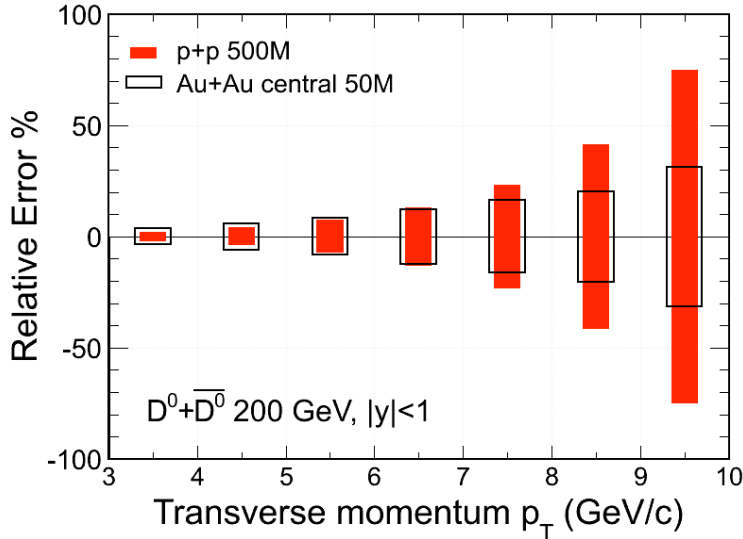


**Figure 5.10** Projected relative uncertainties on the measured  $D^0$   $p_T$  spectra with 500M p+p minimum bias and 50M Au+Au 0-10% central events that can be obtained in Run 14.

## 6. Study of the QCD Phase Diagram in $\sqrt{s_{NN}} \leq 20$ GeV Heavy Ion Collisions

Given the physics considerations discussed below, it is envisioned that the BES Phase – II (BES-II) program be considered to take place soon after 2014 (the need for e-cooling is emphasized in terms of event statistics required in the BES-II program) and fixed target part of the program starts in the year 2014.

### 6.1 Goals and Status of the BES Phase-I (BES-I)

The main objectives of the BES-I at RHIC [1] were the following:

- (a) A search for turn-off of new phenomena already established at higher RHIC energies [2]. The particular observables that was identified as the essential drivers of our run plan are:
  - (i) Constituent-quark-number scaling of  $v_2$
  - (ii) Hadron suppression in central collisions as characterized by the ratio  $R_{CP}$ ;
  - (iii) Untriggered pair correlations in the space of pair separation in azimuth and pseudorapidity;
  - (iv) Local parity violation in strong interactions.
- (b) A search for signatures of a phase transition and a critical point. The particular observables that we have identified as the essential drivers of our run plan are:
  - (i) Elliptic & directed flow for charged particles and for identified protons and pions,;
  - (ii) Azimuthally-sensitive femtoscopy, and
  - (iii) Fluctuation measures, indicated by large jumps in the baryon, charge and strangeness susceptibilities, as a function of system temperature.

Towards achieving these goals, STAR at RHIC collected the following data sets for Au+Au minimum bias collisions, summarized in the table below, for the BES-I.

Year	$\sqrt{s_{NN}}$ (GeV)	$\mu_B$ (MeV)	Events ( $10^6$ )
Run 10	39	112	130.4
Run 11	27	151	70.4
Run 11	19.6	230	35.8
Run 10	11.5	270	11.7
Run 10	7.7	370	4.3
Run 12*	5	550	--

**Table 6.1** BES-I runs in 2010, 2011, and 2012.

\* Test planned in run 12.

Analyses have been ongoing on all of the observables specified in (a) and (b) above. The preliminary results have been reported at QM2011[3], SQM2011 [4], and CPOD2011[5]. Below we present the brief status of three of the new observations from BES-I in the field of relativistic heavy-ion collisions.

**Observation of centrality dependence of chemical freeze-out parameters:** The preliminary STAR results on  $T_{ch}$  and  $\mu_B$  obtained from the ratios of pion, kaon, proton and their anti-particles using a thermal model, THERMUS, are shown in the Figure 6.1. For Au+Au collisions at 39 GeV, like at 200 GeV, we do not observe a centrality dependence of the freeze-out parameters. For 11.5 and 7.7 GeV Au+Au collisions we find both the  $T_{ch}$  and  $\mu_B$  decreases as we go from central to peripheral collisions. *This is a first observation of centrality dependence of chemical freeze-out parameter for relativistic heavy-ion collisions.*

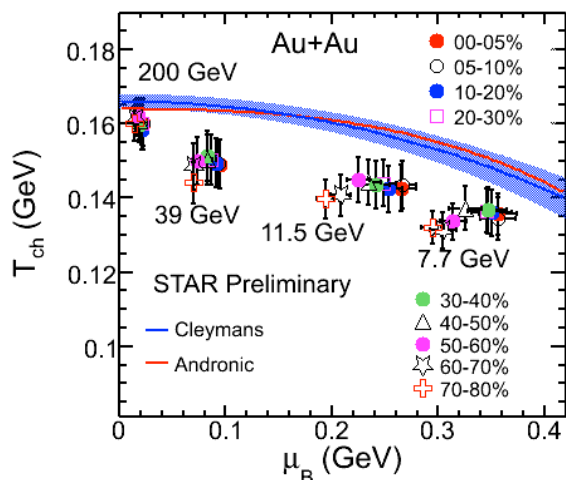


**Figure 6.1** Preliminary results  $T_{ch}$  vs.  $\mu_B$  parameters at chemical freeze-out from Au+Au collisions at 200, 39, 11.5 and 7.7 GeV. Pion, Kaon, proton and their anti-particles are used in the thermal fits. Also shown by blue and red lines are fitting results from [6,7].

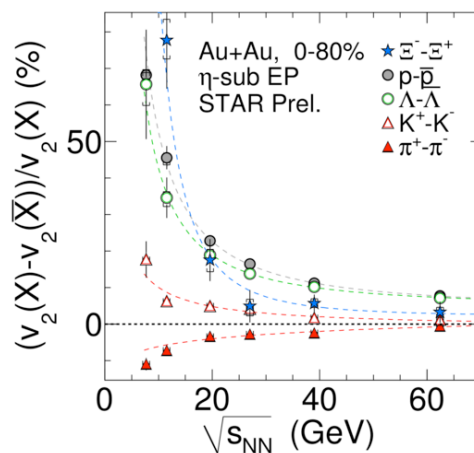


**Figure 6.2** Relative difference between particle and anti-particle  $v_2$  as a function beam energy.

**Particle and anti-particle elliptic flow:** The preliminary STAR results on relative difference between elliptic flow of particle and anti-particles as a function of beam energy are shown in Figure 6.2. We observe that for energies around and below 39 GeV a clear difference is seen between particle and anti-particle  $v_2$ . The difference increases as the beam energy decreases. The difference is more for baryons compared to mesons. The pions reflect an opposite trend compared to the other hadrons. *This is the first observation of a particle and anti-particle  $v_2$  difference in elliptic flow for relativistic heavy-ion collisions.*

**Dynamical charge correlation in heavy-ion collisions:** STAR has used a three particle correlator  $\langle \cos(\phi_1 + \phi_2 - 2\Psi) \rangle$  to search for the signals of Chiral Magnetic effect (CME) in heavy-ion collisions. The difference between the opposite sign correlations and the same sign correlations might be considered as a signal of CME.

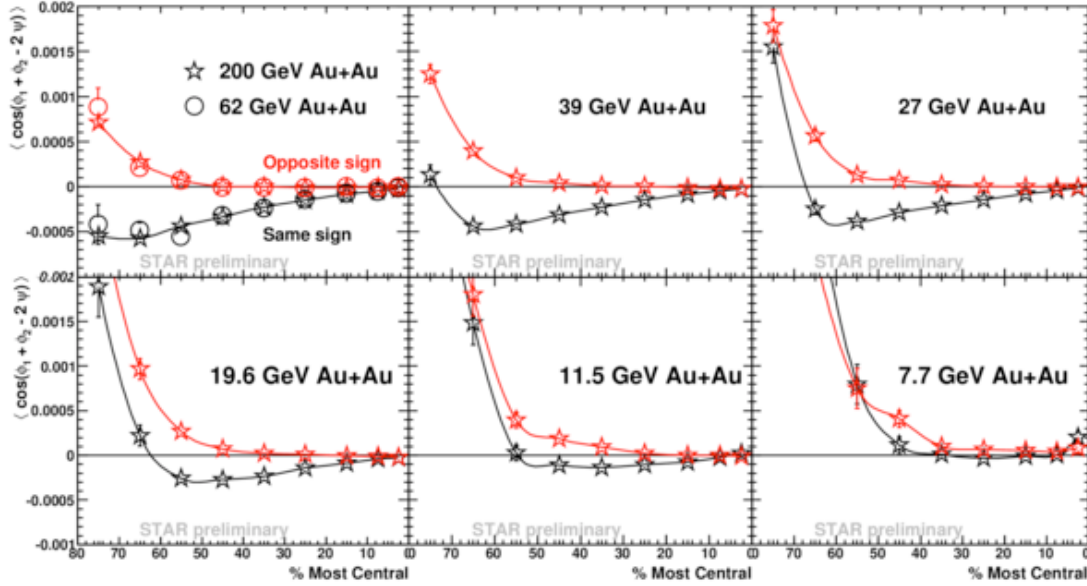


**Figure 6.3** Opposite sign and same sign three particle correlations in Au+Au collisions as a function of collision centrality for various beam energies in BES Phase-I.

Figure 6.3 shows the observable that could be potentially related to the signals of CME in heavy-ion collisions. A clear difference between opposite and same sign correlations are observed at higher energies and it almost vanishes at 7.7 GeV. *This is the first observation of the energy dependence of signals of dynamical charge correlations with respect to reaction plane, which is strongest at 200 GeV and vanishes at 7.7 GeV.*

It is expected that, in the produced nuclear matter, hadronic interactions will be more and more important when beam energy is decreased. These observations suggest the dominance of hadronic interactions over partonic interactions when the collision energy decreases, especially below  $\sqrt{s_{NN}} = 11.5$  Ge.

## 6.2 Selected results from BES-I to motivate Phase – II

**Higher moments of net-proton distributions:** Higher moments of multiplicity distribution of conserved quantities are sensitive to phase transition and critical point effects [8]. Higher the moments, stronger are the dependencies on the correlation length of the system and hence higher is the sensitivity. It is desirable to look at the products of the moments or ratios of the cumulants as they cancel out the volume effect. Net-proton number reflects the net-baryon number, which is a conserved quantity.

The Fig. 6.4 presents the STAR preliminary results on the product of moments and ratio of cumulants for net-proton multiplicity distributions as a function of baryon chemical potential. We find for central 0-5% Au-Au collisions a deviation of the product of moments from Poissonian expectations around  $\mu_B$  corresponding to beam energies of 19.6-27 GeV. The implications of these measurements to understand the QCD phase structure of the phase diagram are not yet resolved. The results show that

there is a need for higher statistics data set at 7.7 and 11.5 GeV as well as data at a new energy point of energy between 11.5 GeV and 19.6 GeV to consolidate the findings. RHIC can provide Au+Au collisions at  $\sqrt{s_{NN}} \approx 15$  GeV.

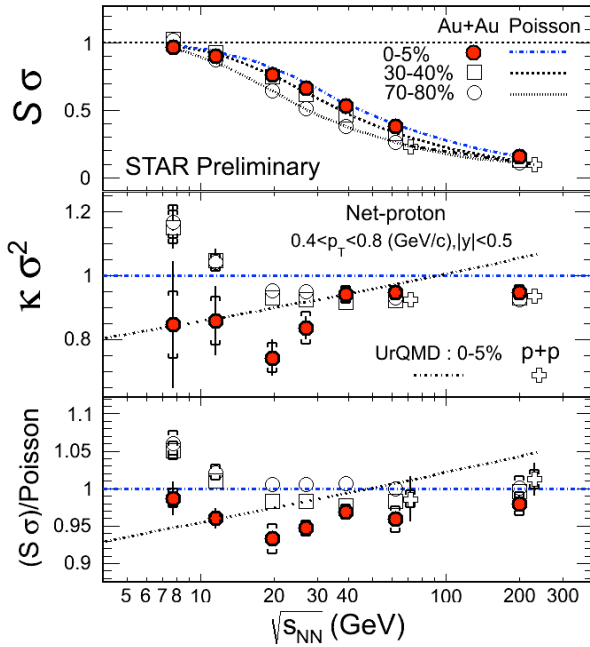


**Figure 6.4** Preliminary results on the product of moments and ratio of cumulants for net-proton multiplicity distribution in Au+Au collisions at mid-rapidity as a function of beam energy. Results from three centrality bins are shown. Dot-dashed-line represents the Poisson reference and the dotted-line shows the results from the transport model UrQMD calculations for the top 5% central collisions.

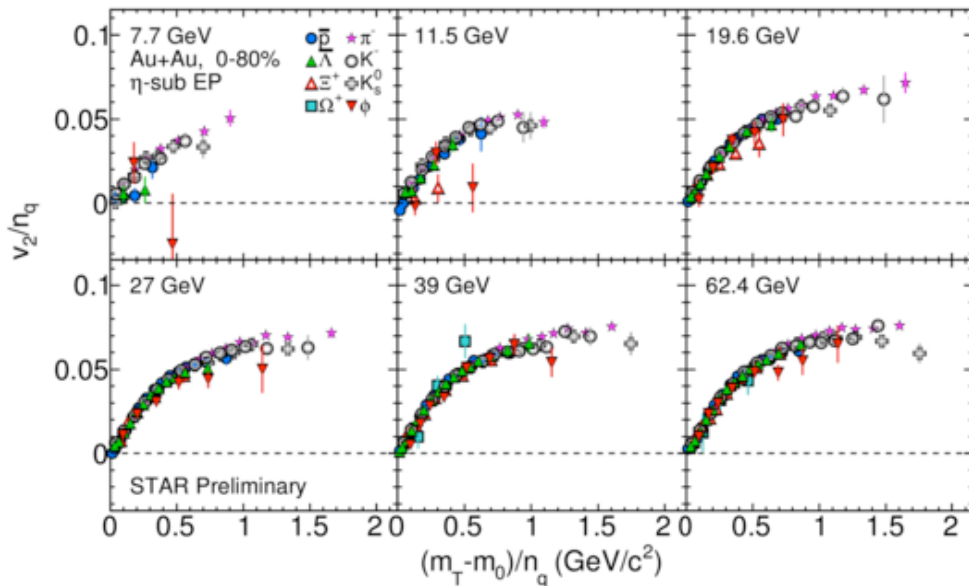
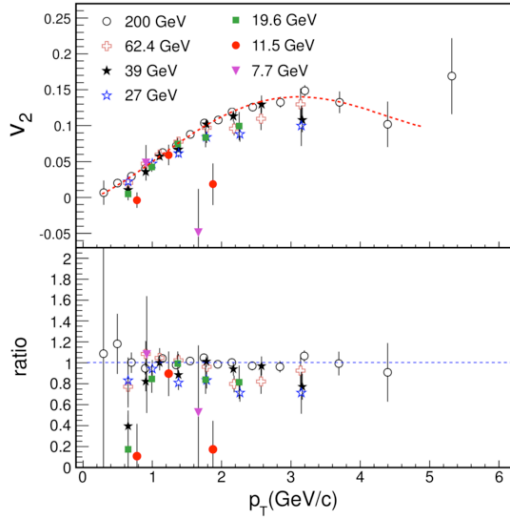


**Figure 6.5** Number of constituent quark scaled elliptic flow of hadrons as a function of transverse kinetic energy scaled by NCQ. The results are for minimum bias Au+Au collisions.

**The  $\phi$ -meson elliptic flow:** One of the striking observations to come out of the top RHIC energies is the observation of scaling of the elliptic flow divided by the number of constituent quark (NCQ) vs. the NCQ scaled kinetic energy, see figure 6.5. This

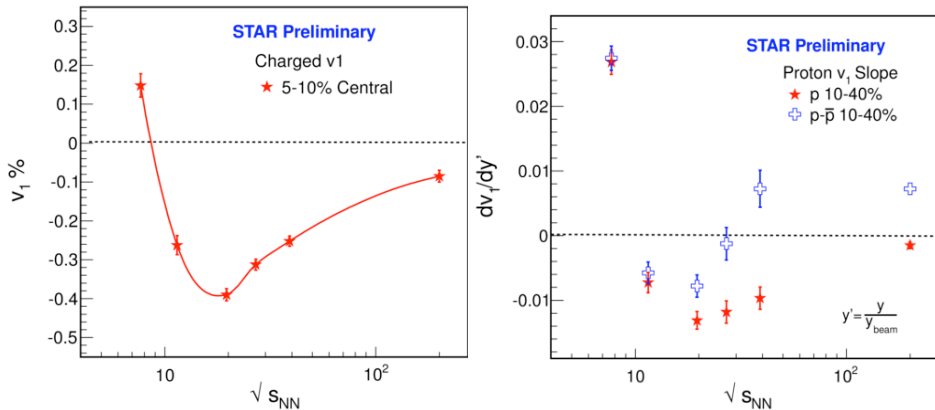
observation has been phenomenologically linked to formation of partonic matter at RHIC [9].

Figure 6.5 shows the results of NCQ transverse kinetic energy scaling from Phase-I of the BES program. Indications (with the available statistics) are that  $\phi$ -mesons as well as Cascade baryons drop off the scaling shown by other produced hadrons at 11.5 GeV.



**Figure 6.6** The  $\phi$ -meson  $v_2$  for various beam energies in minimum bias Au+Au collisions. The bottom panel shows the ratio of  $v_2$  with respect to results at 200 GeV.

In support of the observations in Figure 6.5, we show in Figure 6.6 the  $\phi$ -meson  $v_2$  for collision energies between 200 to 7.7 GeV. The ratio of  $v_2$  with respect to 200 GeV indicates that for beam energies between 200 - 27 GeV, the  $v_2$  are similar to about 10% level. However indications are, that at 11.5 GeV the  $\phi$ -meson  $v_2$  shows a drop in the  $v_2$  values, although the current statistical errors prevent us from drawing a strong conclusion. This emphasizes the need for a high statistics measurement at 7.7 and 11.5 GeV and well as data at a new energy point around 15 GeV.



**Figure 6.7** Left panel: Directed flow of charged hadrons as a function of beam energy for 5-10% central Au+Au collisions. Right panel: Slope of directed flow of protons with respect to rapidity, plotted as a function of beam energy for 10-40% central Au+Au collisions.

**Directed flow:** The rapidity and energy dependence of directed flow ( $v_1$ ) has been proposed to be studied to understand the early time dynamics of the system formed in high energy heavy-ion collisions. A minimum in flow observables and the change in slope of  $v_1$  as a function of rapidity are often related to effects due to first order phase transition.

Figure 6.7 shows a non-monotonic variation of charged hadron  $v_1$  as a function of beam energy for 5-10% central Au+Au collisions. The minimum value of  $v_1$  is reached around 19.6 GeV collisions. Also shown in the right panel sign change in the proton  $v_1$  slope with respect to rapidity as a function of beam energy. At 7.7 GeV for 10-40% collision centrality the slope is positive and it turns negative around 11.5 GeV. The slope reaches a minimum at 19.6 GeV, before going close to zero at 200 GeV.

**Nuclear modification Factor:** Figure 6.8 shows the STAR preliminary results on nuclear modification factor for strange hadrons in BES Phase-I energies. We can see suppression effects for  $\phi$ -mesons and Kaons at 39 GeV. Within the current  $p_T$  reach no such suppression effects are seen at 11.5 and 7.7 GeV. With the quoted statistical errors a baryon-meson separation is also observed at 39 GeV. No such indications are seen from the data at 11.5 and 7.7 GeV. A higher statistics data set at 7.7 and 11.5 is needed to extend the  $p_T$  range.

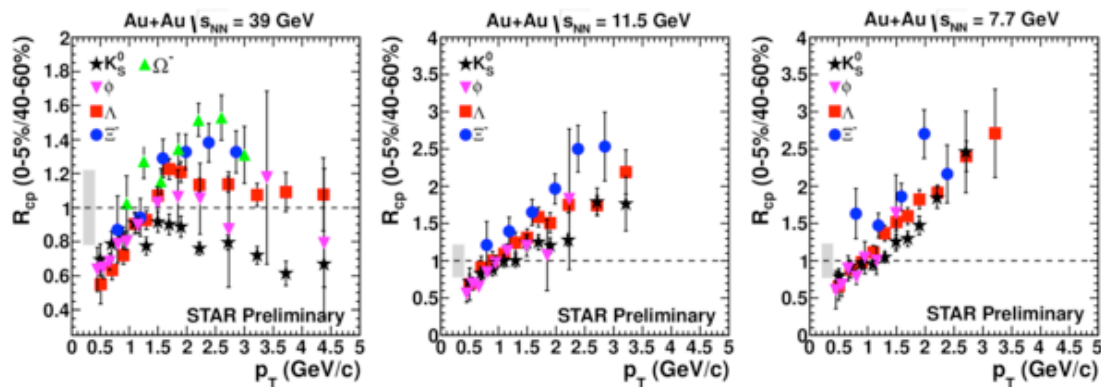


**Figure 6.8** Nuclear modification factor for strange hadrons as a function of  $p_T$  for three BES energies.

### 6.3 Proposals for the BES Phase – II

**BES Phase-II Program:** During the BES Phase-I campaigning, we have collected sizable data sets for Au+Au collisions at 7.7, 11.5, 19.6, 27 and 39 GeV. However, for several important observables, such as the phi-meson  $v_2$  (Figs. 6.5 and 6.6), net-proton higher moments (Fig. 6.4), the statistics are not sufficient, especially at the lower collision energies. Adding an electron cooling device at the RHIC, the luminosity for collisions below  $\sqrt{s_{NN}} = 20$  GeV will be greatly increased. As shown in figure 6.9, simulation results indicate that at 7 and 20 GeV, the expected increasing factors are about 3-5 and 10, respectively [13]. It was reported before that using electron cooling to

counteract IBS at these energies and providing longer physics stores would increase luminosity significantly, with the limitation imposed by the space-charge effects. Recently [14], it was shown that an additional improvement in luminosity may be possible by operating with longer bunches at the space-charge limit in a collider, which further extends benefits from cooling at low energies. Overall improvement from cooling could be about 10-fold gain in total luminosity with significant improvement of luminosity even for a short vertex cut of the detector.

The increasing luminosity from the e-cooling will allow precision measurements of the above important observables for exploring the QCD phase diagram around  $\mu_B = 400 - 200$  MeV region. In addition, the increased luminosity will make the measurements of rare probes such as the dilepton at the  $\sqrt{s_{NN}} = 20$  GeV region meaningful.

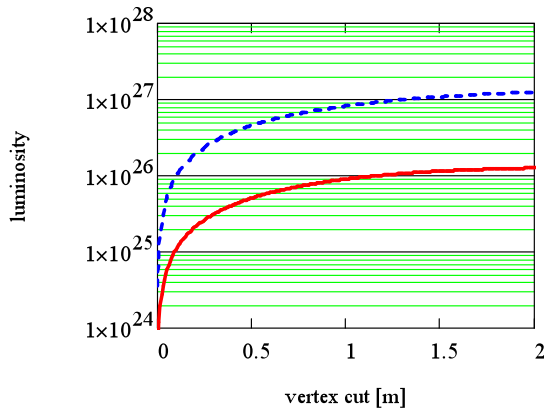


**Figure 6.9** Average luminosity for 111 bunches of Au ions in RHIC at  $\gamma=10.5$  and space-charge tune spread  $\Delta Q_{sc}=0.05$ : 1) with electron cooling and long bunches ( $\sigma_s=3$  m,  $\beta^*=1$  m,  $\epsilon_{n,95\%}=5$   $\mu\text{m}$ ,  $N_i=2.1e9$ ) - blue, dash curve; 2) without cooling ( $\sigma_s=1$  m,  $\beta^*=3$  m,  $\epsilon_{n,95\%}=15$   $\mu\text{m}$ ,  $N_i=2.1e9$ ) – red, solid lower curve. Here, maximum luminosity without cooling was divided by a factor of 3 to account for luminosity lifetime due to IBS and time between refills. Taken from [14].

Driven by the physics and the preliminary BES-I results, we propose heavy ion collisions, including both Au+Au and U+U collisions, at energies below  $\sqrt{s_{NN}} = 20$  GeV in BES-II.

$\sqrt{s_{NN}}$ (GeV)	$\mu_B$ (MeV)	Collected events ( $10^6$ )	Requested events ( $10^6$ )
Au+Au: 19.6	230	36	150*
Au+Au: 15	256	---	150
Au+Au: 11.5	270	11	50
Au+Au: 7.7	370	5	70
U+U: $\sim 20$	$\sim 230$	--	100

**Table 6.2** Requested event statistics for BES-II program.

\* Based on dielectron measurements discussed below.

**Note on proposed RHIC running for U+U collisions at 20 GeV:** Some important observations (Deviations from NCQ scaling, change in nuclear modification factors, Deviations of fluctuations from Poissonian expectations, minimum in  $v_1$  measurements etc ...) are being observed from the BES data analysis around 20 GeV collisions. U+U at 20 GeV with its different configurations (as it is a deformed nuclei) allows extending the energy densities attained and  $v_2$  values to about 30% higher than in a similar configurations with Au+Au collisions. Hence the signals could be more

pronounced for U+U collisions at 20 GeV. However a higher event statistics would be needed for U+U minimum bias collisions relative to Au+Au minimum bias collisions in order to select the proper geometrical collision configurations that would give higher densities.

**Rare probes in the BES Phase-II Program:** E-cooling is also beneficial for STAR program at higher end of the BES energies. Below we discuss two measurements from BES-I in support of this argument.

**(1) Dilepton production:** Dielectron distribution is an important bulk-penetrating probe that providing valuable information on the collision history. Due to its physics origin, the rates of the production is low thus requires a large event samples. During the BES phase-I, we collected about  $36 \times 10^6$  Au+Au collisions at 19.6 GeV but the statistics errors are large for dielectron mass distribution.

Mass (GeV/c <sup>2</sup> )	Percentage statistical error (%)
0.2	17
0.325	42
0.5	39
0.66	46
0.745	50

**Table 6.3** Current estimates of the typical statistical errors for several mass bins of the dielectron measurement in  $\sqrt{s_{NN}} = 19.6$  GeV Au+Au collisions.

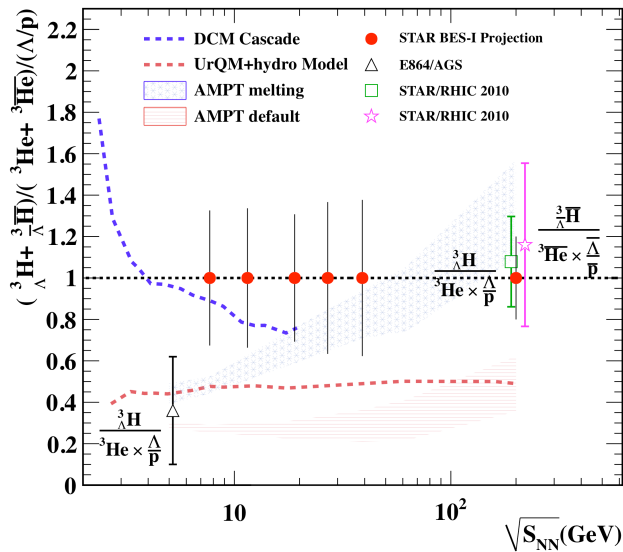


**Figure 6.10** Strangeness population factor for Au+Au collisions at various beam energies. The projected statistic errors from BES-I are shown.

Figure 6.10 shows the projections of the statistics errors of strangeness population factor for Au+Au collisions at BES-I energies. The projections are compared to models with and without partonic interactions. The statistical errors in current data are large. A factor of 10 more event statistics (shown in Table of section I) is needed to have a firm conclusion from this measurement.

In order to have comparable statistical errors as for the SPS measurement by CERES, at least a factor of 4 more event statistics is needed. In order to have a statistical error of about 10% or less in above mass bins, we need a factor of 10 more event statistics. Further dilepton spectra excitation function is expected to provide information on the importance of the baryonic component of the medium to the medium effects on vector meson production [10]. This clearly shows the need for e-cooling to have high precision dilepton measurements at BES energies in STAR.

**(2) Strangeness population factor  $S_3$ :** With the discovery of the anti-hypertriton and measurements of hypertriton in STAR [11], a new observable sensitive to quark hadron phase transition has been proposed. It is the ratio of the hyper-triton yields to Helium-3 yields scaled by the ratio of lambda to proton ratio. This Strangeness Population factor ( $S_3$ ) is believed to have very different values in a partonic system compared to a hadronic system, see figure 6.10.

## 6.4 Proposal for STAR in Fixed-Target Mode

**Physics goals and event statistics:** The main goal of the fixed-target mode running is to extend the range of accessible baryon chemical potentials from the current maximum of about  $\mu_B \sim 400$  MeV up to  $\sim 800$  MeV, corresponding to the collision energy  $\sqrt{s_{NN}} \sim 2.5$  GeV, in the QCD phase diagram. The physics motivations are similar to those proposed for the BES Phase – I, however the fixed-target mode focuses on the physics goal that is expected at the lowest energies – i.e. evidence of the first order phase transition through identification of the softest point. At collision energies well below the phase boundary, we expect systems to be created which generate and respond to pressure following a pure hadron gas equation of state. As the collision energy is increased, we create systems that can enter the mixed phase region. The phase coexistence region is thermodynamically unstable (spinodal region) and exhibits very low compressibility (softening of the equation of state). Systems that have enough energy to achieve the onset of deconfinement will spent the maximum time in the spinodal region (softest point). As the collision energy increases further, the “turning point” of the phase trajectory moves deeper inside the plasma region, and one expects that the system to generate and respond to pressure following a partonic equation of state.

The average compressibility of the system can be inferred by studying observables which respond to pressure. We propose to study the elliptic flow, the directed flow, and the azimuthal HBT. Figure 6.12 shows some results from the BES-I data as well as from other experiments. In the left panel, the unidentified charged particle flow is shown as a function of collision energy. The arrows are drawn in to indicate that there is an apparent inflection point in the development of flow with collision energy, which might be an indication of a change in the equation of state. However, it should be noted that this interpretation relies on comparing results from two different experiments. Without the recent STAR BES-I result, there have appeared to be a smooth development from E895 to NA49. It is important to better characterize this transition

and to identify the precise location of the inflection point. In the right panel, the final coordinate space eccentricity is shown as a function of beam energy. The lowest energy points show a higher than expected freeze-out eccentricity. This enhancement in the eccentricity is associated with the tilting of the source, which is a response to the directed flow. The drop in the eccentricity indicates a reduction in the tilt which may be associated with a change in the equation of state. It should also be noted that the directed flow shown in figure 6.7 exhibits a transition from positive to negative above 7.7 GeV.

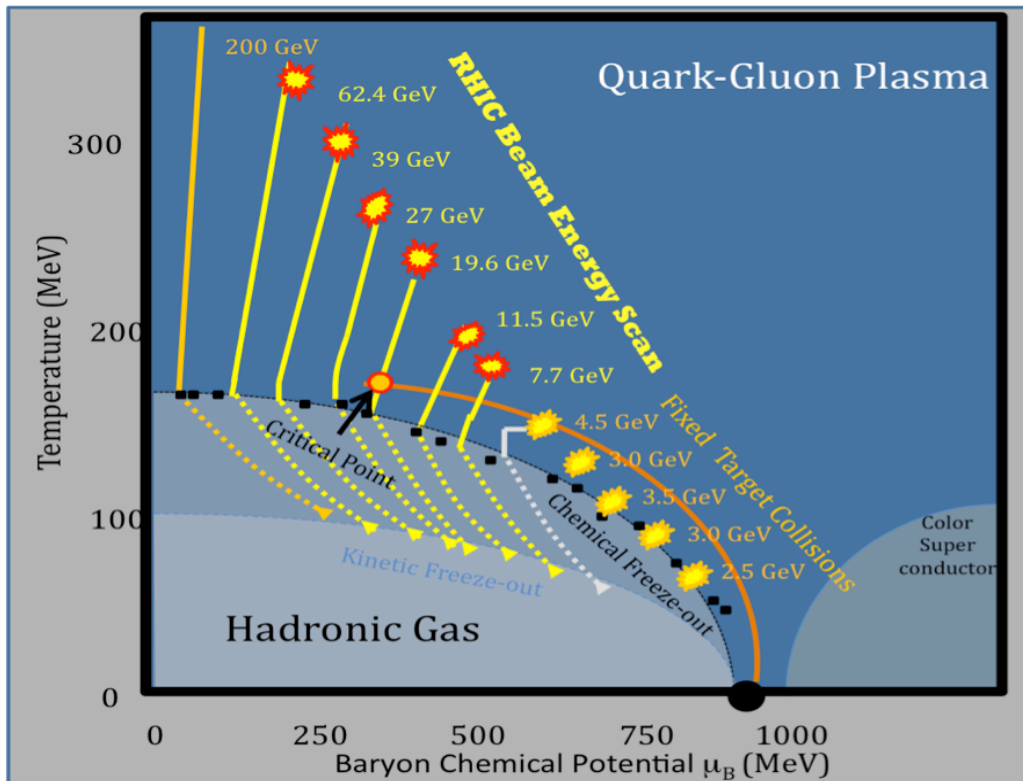


**Figure 6.11** A cartoon of the phase diagram of nuclear matter showing the fixed target points.

The results shown in figures 6.7 and 6.12 point to the importance the 7.7 GeV data point. It should be noted that NA49 has reported signatures of the onset of deconfinement near  $\sqrt{s_{NN}} = 7.7$  GeV[15]. It is of major importance for the field to confirm or falsify this NA49 result. In order to do this, one needs to take data above and below the reported transition. The importance of studying systems at or slightly below this threshold was already recognized in the BES-I proposal [16];  $\sqrt{s_{NN}} = 7.7$  GeV was not expected to be low enough ( $m_B \sim 400$  MeV) and therefore one of the energies proposed was 5 GeV ( $\mu_B \sim 530$  MeV).

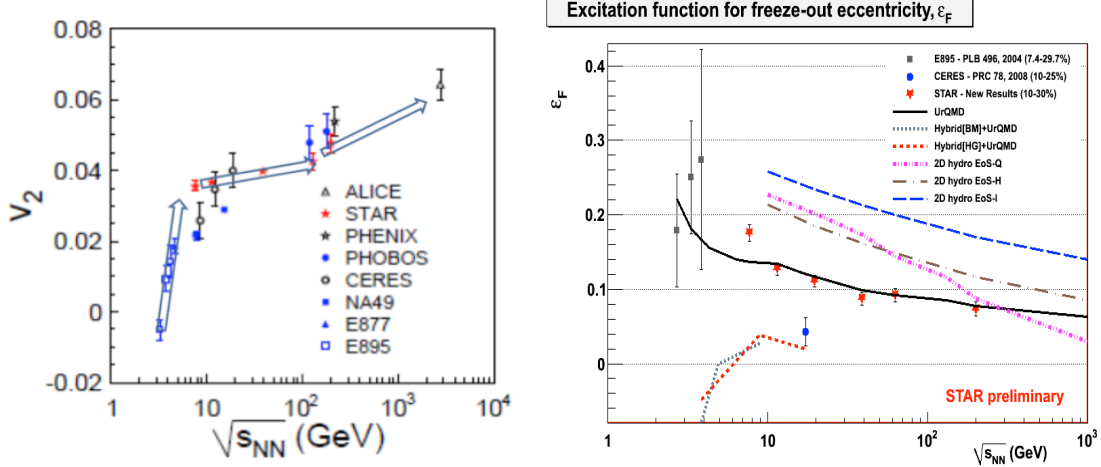


**Figure 6.12** Left panel: elliptic flow of charged hadrons as a function of beam energy for 20-30% central Au+Au collisions. Right panel: The freeze-out coordinate space eccentricity as measured through azimuthal HBT plotted as a function of collision energy for 10-30% central Au+Au collisions.

The extension of the beam energy scan to lower collision energies and to a baryon chemical potential of 800 MeV can be accomplished by use of a fixed target mounted inside RHIC beam pipe. The fixed-target data-taking can proceed with minimal or no impact on RHIC operations in collider mode. Collisions between injection-energy gold ions and a fixed gold target will allow the study of  $\sqrt{s_{NN}} = 4.5$  GeV. The proposed 15 GeV colliding beams will provide  $\sqrt{s_{NN}} = 4.0$  GeV fixed target collisions. The already developed sub-injection energy beams at RHIC, 11.5 and 7.7 GeV, will provide fixed target collisions at energies of  $\sqrt{s_{NN}} = 3.5$  and 3.0 GeV, respectively. And the 5.0 GeV collider test will provide 2.5 GeV fixed target collisions.

Collider Mode Energy (GeV)	5	7.7	11.5	15	19.6
Fixed Target $\sqrt{s_{NN}}$ (GeV)	2.5	3.0	3.5	4.0	4.5
Fixed Target $\mu_B$ (MeV)	775	720	670	625	585
Fixed Target $y_{CM}$ (Acceptance 0.0 to 1.7)	0.82	1.05	1.25	1.39	1.52
<b>Observables</b>	<b>Required Event Statistics (<math>10^6</math>)</b>				
$v_2$ (up to $\sim 1.5$ GeV/c)	1.1	0.9	0.8	0.7	0.6
$v_1$ (Protons and Pions)	1.0	0.8	0.7	0.6	0.5
Azimuthally sensitive HBT (pions)	20	15	13	11	10

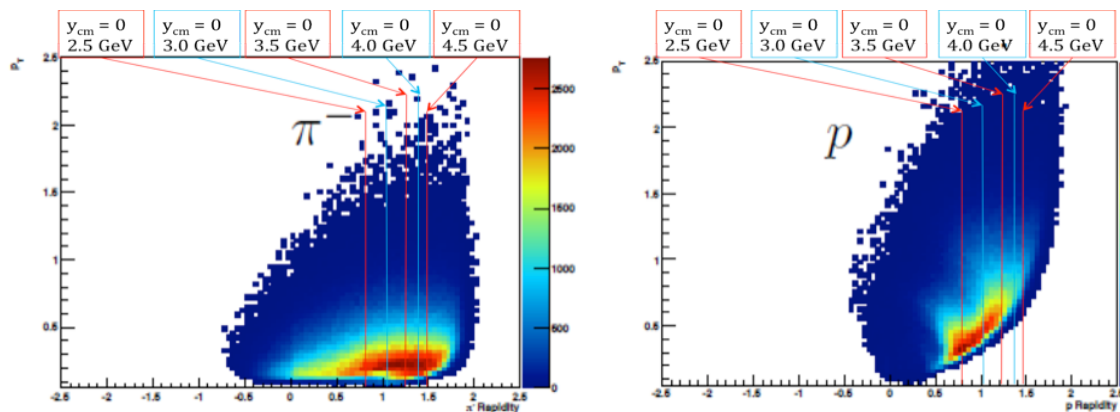
**Table 6.4** The fixed-target request.

Table 6.4 gives the estimated event statistics needed to carry out various physics analysis for a typical fixed target mode of running at all of the energies considered.

**STAR configuration for fixed target plan:** For the fixed-target program for STAR, we propose to install an annular 1% gold target inside the STAR beam pipe. The target will be located about 2 meters from the center of the STAR detector. It will be mounted within an aluminum sleeve that fits snugly inside a section of the STAR beam pipe that is made of 3 inch (7.62 cm) O.D. aluminum pipe with a 60 mil wall thickness. This mounting fixture will be designed to slide inside the existing STAR beam pipe. The target will be installed during the summer 2013 shutdown when the STAR detector is rolled into the assembly building.

During BUR14 gold running, fixed-target events will be taken at injection energy at the beginning of each fill. This will happen concurrently with Au+Au data-taking at 200 GeV (i.e. every store prior to accelerating Au ions to 200 GeV). We will turn the STAR detector on prior to injection of the blue beam; we will take data using collisions from the halo of the blue beam while it is circulating at injection energy. When the collider starts injection of the yellow beam, we will power the detectors down to be safe prior to the ramp to full energy. This will allow about 5 minutes of injection energy fixed-target data per fill. With RHIC refilling every four hours, we can expect about 30 minutes of data per day, which corresponds to up to 1.5 million fixed target collisions per day. Assuming a five-week 200 GeV Au+Au run, we could acquire up to 5 weeks x 7 days/week x 1.5 M events/day = 52 M fixed-target events.

The BES-II program, which is detailed above, requests Au+Au collisions at 19.6, 15, 11.5 and 7.7 after electron cooling upgrade. The gold target will be installed for these runs, allowing fixed target collisions at 4.5, 4.0, 3.5, and 3.0 GeV respectively. These events can be triggered upon and recorded without reducing the number of collider events recorded as the expected luminosities will not fill the DAQ bandwidth.



**Figure 6.12** Left panel: Pions accepted from Au+Al fixed-target events taken as background during BES-I. The various vertical lines indicate the center of mass rapidity for the various collision energies proposed for the fixed target program. Right panel: same as left, except for protons. (Note: the kaon acceptance would be intermediate to pions and protons, however the center of mass boost makes kaon ID challenging.)

**Detector capabilities for the physics program:** The fixed target will be positioned two meters from the center of the TPC. This will provide the best acceptance of the TPC and TOF systems for mid-rapidity particles. The performance of STAR for

collisions offset fixed target collisions has been studied using background Au+beampipe collisions which were recorded during the BES-I running. The momentum resolution of STAR for offset fixed target tracks has not been seen to be significantly different from standard  $V_z=0$  collider events.

The fixed target configuration provides a challenge for particle identification. The boost to the center-of-mass moves particles with low transverse mass and rapidities near mid-rapidity into the region for which PID through  $dE/dx$  becomes challenging. This issue is most critical for the mid-rapidity charged kaons, which will not be identifiable using  $dE/dx$  in the fixed target program.

For the offset vertices of the fixed-target program, the TPC tracking efficiency remains high for  $\eta$  from 0 to 1.8. The acceptances for fixed-target running are shown in the figure below. The  $\eta$  acceptance does create a low  $p_T$  acceptance threshold for kaons and protons.

## References:

1. STAR BES Proposal, STAR Note SN-0493 (2009).
2. J. Adams et al., (STAR Collaboration), Nucl. Phys. A 757 (2005) 102.
3. B. Mohanty (For STAR Collaboration), J. Phys. G 38 (2011) 124023.
4. S. Kabana (For STAR Collaboration), arXiv:1203.1814.
5. A. Schmah (For STAR Collaboration), arXiv: 1202.2389.
6. J. Cleymans et al., Phys. Rev. C 73 (2006) 034905.
7. A. Andronic et al., Nucl. Phys. A 837 (2010) 65.
8. M. M. Aggarwal et al., (STAR Collaboration), Phys. Rev. Lett. 105 (2010) 022302.
9. B. I. Abelev et al., (STAR Collaboration), Phys. Rev. Lett. 99 (2007) 112301; B. Mohanty, N. Xu, J. Phys. G 36 (2009) 064022.
10. G. David, R. Rapp, Z. Xu, Phys. Rept. 462 (2008) 176.
11. B. I. Abelev et al., (STAR Collaboration), Science 328 (2010) 58.
12. STAR fixed target proposal, STAR Note 2012.
13. A. Fedotov, and W. Fischer, Private communications, 2012.
14. A. Fedotov and M. Blaskiewicz, "Potential for Luminosity Improvement for Low-Energy RHIC Operation with Long Bunches", BNL C-AD Tech Note: C-A/AP/449 (February 10, 2012).
15. NA49 Collaboration, Phys. Rev. C 77, 024903 (2008).
16. STAR BES Proposal, STAR Note SN-0493 (2009).